Contents lists available at ScienceDirect

Electrochimica Acta

From lithium to potassium: Comparison of cations in poly(ethylene oxide)-based block copolymer electrolytes for solid-state alkali metal batteries

Anna D. Khudyshkina [a], Andreas J. Butzelaar [b], Yiran Guo [a], Maxi Hoffmann [b], Thomas Bergfeldt [c], Mareen Schaller [a], Sylvio Indris [a], Manfred Wilhelm [b], Patrick Théato [b,d,*], Fabian Jeschull [a,*]

[a] Karlsruhe Institute of Technology (KIT), Institute for Applied Materials - Energy Storage Systems (IAM-ESS), Hermann-von-Helmholtz-Platz 1, 76344 Eggenstein-Leopoldshafen, Germany
[b] Karlsruhe Institute of Technology (KIT), Institute for Chemical Technology and Polymer Chemistry (ITCP), Engesserstraße 18, 76131 Karlsruhe, Germany
[c] Karlsruhe Institute of Technology (KIT), Institute for Applied Materials – Applied Materials Physics (IAM-AWP), Hermann-von-Helmholtz-Platz 1, 76344 Eggenstein-Leopoldshafen, Germany
[d] Karlsruhe Institute of Technology (KIT), Soft Matter Synthesis Laboratory - Institute for Biological Interfaces III (IBG-3), Hermann-von-Helmholtz-Platz 1, 76344 Eggenstein-Leopoldshafen, Germany

ARTICLE INFO

ABSTRACT

Liquid electrolytes (LEs) commonly show severe side reactions at the electrode-electrolyte interface, especially with alkali metal anodes, leading to rapid capacity fade of metal-ion batteries. Solid polymer electrolytes (SPEs), however, contribute to the suppression of side reactions due to their inherent inertness and high mechanical strength, providing long-term stable battery operation. Herein, we investigated physical and electrochemical properties of SPEs based on our previously reported microphase-separated poly(vinyl benzyl methoxy poly (ethylene oxide) ether)-*block*-polystyrene block copolymer (PVBmPEO-*b*-PS) with different alkali metal ions (A^+ = Li^+, Na^+ or K^+) and their use in the respective metal batteries, showing the potential for the transition from lithium to post-lithium batteries. Rheological and thermal properties as well as ion transport in the SPEs with different bis(trifluoromethanesulfonyl)imide (TFSI) salts concentrations revealed similar shear storage moduli (G') for the investigated SPEs, while the lowest glass transition temperatures (T_g) were found for KTFSI-based films. By contrast, the highest total ionic conductivity was found for the LiTFSI-based SPEs. To quantify the A^+ transference numbers (T_A^+), the Bruce-Vincent method and pulsed-field gradient (PFG) NMR were conducted, revealing significant challenges for T_A^+ determination of post-Li systems. Further, the examination of the interfacial stability of SPE/A interfaces by conducting plating/stripping experiments revealed significantly higher resistances for sodium- and potassium-based systems in comparison to their lithium-based counterpart. Nonetheless, A-metal/SPE/cathode cells with PVBmPEO-*b*-PS-based Na- and K-SPEs with the Prussian Blue analogues (PBAs, $Na_{2-x}Fe[Fe(CN)_6]$ and $K_{2-x}Fe[Fe(CN)_6]$) positive electrodes and the respective alkali metal negative electrodes enabled cycling at elevated temperature of 55 °C. Herein, both sodium and potassium metal batteries exhibited stable cycling with capacity retentions of 73% over 100 cycles for the Na-cell, and 94% over the same cycle number for the K-cell, (and a high coulombic efficiency (CE) of 98% at the 100th cycle).

1. Introduction

In recent years, the growing demand for rechargeable batteries with high energy density has promoted the evolution of conventional lithium-based batteries as well as the search for complementary post-Li technologies. Batteries based on alternative alkali metals (A), particularly sodium and potassium, are advantageous over lithium in terms of their natural abundance and higher availability, which is expected to make a positive impact on materials and battery cost, especially with regard to large-scale stationary energy storage applications [1–4]. On

---

the other hand, both Na and K possess higher atomic masses than Li, which generally results in inferior volumetric and gravimetric capacities of corresponding batteries [5]. Common cathodes for both Na- and K-based batteries are Prussian Blue analogues, i.e., PBAs, with the general formula $A_2M[Fe(CN)_6]$ (where M represents a transition metal, e.g. Fe or Mn) [6,7], or polyanionic compounds (e.g., $A_3V_2(PO_4)_3$) [8,9], which exhibit high average potentials of 3.5–4.3 V vs. A^+/A [10]. In combination with a metallic anode, the cell voltage can be maximized. This, however, is associated with a high reactivity of electrolyte components towards the respective alkali metals, resulting in low coulombic efficiencies (CE) and rapid cell failure due to dendrite growth toward electrolyte components [11–13]. Compared to liquid electrolytes (LEs), solid polymer electrolytes (SPEs) typically exhibit a broader (electrochemical) stability window [14–16] and may suppress metallic dendrite penetration because of their better mechanical properties, e.g. higher mechanical integrity [17–19].

However, as a result of their generally low room temperature ionic conductivity [20], SPEs, especially those based on poly(ethylene oxide) (PEO), are typically operated above the melting point of the PEO phase, leading to a significant loss of their mechanical strength. Furthermore, in our previous study, the rheological data demonstrated that compositions comprising PEO and potassium bis(trifluoromethanesulfonyl) imide (KTFSI) in the range of EO:K molar ratios from 16:1 to 12:1 displayed a liquid-like behavior (i.e., shear loss modulus dominating over shear storage modulus) in the temperature range from 35 to 65 °C [21]. Their fluid-like character rendered them better ionic conductors below the melting point, but unsuitable as separators between the cathode and anode in the cell stack.

In an attempt to merge high mechanical stability with improved ionic conductivity, in this study we use our previously introduced poly (vinyl benzyl methoxy poly(ethylene oxide) ether)-*block*-polystyrene block copolymer [22] (PVBmPEO-*b*-PS, further shortened to BP as block copolymer) as a host polymer material for SPEs. In the microphase-separated BP, the polar PEO-based block enables ion transport, while the non-polar rigid PS block maintains the mechanical stiffness of the SPE-film over a wide temperature range, above the melting point of the PEO phase and below the T_g of PS. Using a combination of rheological and electrochemical characterization techniques, we will demonstrate that the block copolymer approach is a viable path to contain ionically well-conducting polymer-salt compositions in a rigid matrix, while benefiting from considerably improved mechanical properties.

In addition, it is our aim in this study to draw a comprehensive picture of the change in SPEs properties when moving from Li- to post-Li systems, i.e., when Li^+ cation is replaced by either Na^+ or K^+, while maintaining the TFSI$^-$ anion. For PEO-ATFSI (A = Li, Na, K) Oteo et al. [23] recently reported similar ionic conductivities but a higher Na^+ transference number (T_{Na}^+), than for the Li-system (T_K^+ was not determined). Earlier studies on the cation coordination of PEO-AXE complexes (A = Li, Na, K, Rb; X = SCN, ClO$_4$, CF$_3$SO$_3$) suggested that the coordination number and PEO chain conformation change for cation radii larger than that of Na$^+$ [24,25]. As a result, weaker coordination strength of larger A^+ with both the polymer chain and the anion can be suspected, which in turn may allow for higher cation transport in the polymer matrix [26]. We have approached this question, using polarization techniques in symmetrical alkali metal cells as well as pulsed-field gradient nuclear magnetic resonance spectroscopy (PFG NMR). As we have encountered individual limitations with each of these techniques, selected BP-based electrolytes (BPEs) with NaTFSI and KTFSI were studied in alkali metal/SPE/Prussian white cell configurations to highlight potentials and practical limitations with block copolymer-based polymer electrolytes for post-Li battery applications.

2. Experimental section

2.1. Materials

Sodium hydride (60 wt.% dispersion in mineral oil, Sigma-Aldrich), poly(ethylene oxide) monomethyl ether (mPEO2000 equals to M_n = 2000 g mol^{-1}, TCI), 4-vinylbenzyl chloride (90 wt.%, Sigma-Aldrich), 2-(dodecylthiocarbonothioylthio)−2-methylpropionic acid (98 wt.%, Sigma-Aldrich) were used as received. Styrene (99 wt.%, Acros) was passed through basic alumina oxide prior to use. Alkali metal (A) bis (trifluoromethanesulfonyl)imide salts (ATFSI) with A = Li, (99+ wt.%, Solvionic), A = Na (99.5 wt.%, Solvionic), A = K (99.5 wt.%, Solvionic) were dried at 110 °C for 12 h under vacuum (10^{-3} mbar) and were subsequently stored in an Ar-filled glovebox under inert atmosphere (H$_2$O < 0.1 ppm, O$_2$ < 0.1 ppm). All other solvents and reagents were of analytical grade or higher and were used without further purification.

2.2. Block copolymer synthesis (PVBmPEO-b-PS)

Poly(vinyl benzyl methoxy poly(ethylene oxide) ether)-*block*-polystyrene block copolymer (PVBmPEO-*b*-PS, further shortened to BP) was synthesized by reversible addition-fragmentation chain-transfer (RAFT) polymerization, as described previously[22].

2.3. Synthesis and characterization of K_2Fe[Fe(CN)_6]

Potassium iron hexacyanoferrate K$_{1.90}$Fe[Fe(CN)$_6$] × zH$_2$O (KFF) was synthesized as previously described in ref. [21]. The material composition and water content was determined by inductive coupled plasma optical emission spectroscopy (ICP-OES) and thermogravimetric analysis (TGA), respectively, as stated below.

2.3.1. ICP-OES
Elemental analysis of KFF was performed on iCAP 7600DUO (ThermoFisher Scientific). For the analysis, 4–8 mg of the samples (weighing accuracy ± 0.04 mg) were dissolved in 25 ml hydrochloric acid for 4 h in a graphite oven (EasyDigest, Analab). The analysis of the elements was accomplished with four different calibration solutions and an internal standard (*Sc*). The range of the calibration solutions did not exceed a decade. The two (for K and Na) or three (for Fe) major wavelengths of the elements have been used for calculation.

2.3.2. Thermogravimetric analysis (TGA)
TGA of KFF was conducted on a NETZSCH STA 449 C system in an argon atmosphere with a flow rate of 300 ml min^{-1}. For the measurement, 11 mg of the sample was placed into an aluminum pan and subsequently heated from 35 to 510 °C with a heating rate of 5 K min^{-1}.

2.4. Solid polymer electrolyte (SPE) preparation and characterization

Prior to the SPE film preparation, the PVBmPEO-*b*-PS block copolymer was dried at 80 °C under vacuum (10^{-3} mbar) overnight and transferred to the Ar-filled glovebox, where all following procedures were carried out under an inert atmosphere (H$_2$O < 0.1 ppm, O$_2$ < 0.1 ppm). The predefined amounts of the polymer and ATFSI salts, corresponding to the molar ratios of ethylene oxide (EO):A = 20:1, 15:1, 10:1, were dissolved in acetonitrile (99.8 wt.%, Sigma-Aldrich). Subsequently, the solutions were poured into Teflon molds, followed by acetonitrile evaporation at 60 °C. The obtained films were dried and simultaneously annealed at 110 °C for 36 h under vacuum (10^{-3} mbar). The derived films with a thickness of ~100 μm were further used for all measurements.

2.4.1. Differential scanning calorimetry (DSC)
A DSC Q200 (TA Instruments) system was used to conduct the measurements in the temperature range from −70 to 150 °C with a scan

rate of 10 K min^{-1}. Subsequently, the heat flow was normalized by sample mass.

2.4.2. Oscillatory rheology

Rheological measurements were performed on a strain-controlled ARES G2 (TA Instruments) rheometer via small amplitude oscillatory shear (SAOS) experiments from 0.1 to 100 rad s^{-1} at 25 °C and 55 °C under nitrogen using an 8 mm parallel plate geometry and shear strains from 0.1 to 1%. The samples with a diameter of 8 mm and a thickness of 0.5 mm were prepared from the films obtained by the SPE preparation.

2.4.3. Determination of ionic conductivity

SPE films with a diameter of 10 mm and a thickness of ~100 μm were sandwiched between two stainless steel electrodes in CR2032-type coin cells. The electrolyte conductivity was determined from electrochemical impedance spectroscopy (EIS) measurements using a VSP multichannel potentiostat (BioLogic Science Instruments) over a frequency range from 1 MHz to 500 mHz (and reverse) and a voltage amplitude of 10 mV. The heating-cooling cycle with intermittent EIS measurements was carried out as follows: In the preconditioning the cells were heated to a constant temperature of 60 °C for 12 h before the cells were allowed to cool back to room temperature. After another 12 h, the temperature was decreased to 5 °C and the cells were briefly equilibrated for 50 min at this temperature. After equilibration three EIS measurement were carried out (each measurement includes forward and backward scan). The temperature was then increased in 10 °C steps to 85 °C with a heating rate of 1 °C min^{-1} over 10 min and a subsequent 50 min temperature hold in each step, before EIS spectra were recorded. At a temperature of 85 °C, the heating profile was reversed and gradually cooled down to 5 °C in the same manner. The bulk electrolyte resistance (R_b) was extracted from the Nyquist plot, and ionic conductivity (σ) was calculated according to Eq. (1):

$$\sigma = \frac{1}{R_b} \cdot \frac{l}{A} \tag{1}$$

where l represents the thickness, and A represents the area of a SPE film.

2.4.4. Transference number (T_A^+) measurements

2.4.4.1. Bruce-vincent method.
The measurements of the transference number T_A^+ were performed on a VMP-300 potentiostat (BioLogic Science Instruments) at 55 °C. For the measurements, symmetrical A/SPE/A coin cells were assembled. BP-based electrolytes (BPE)$_{15}$-ATFSI$_1$ with a molar ratio of EO:A = 15:1 were prepared as described in Section 2.4. The electrolyte discs with a thickness of ~100 μm and a diameter of 8 mm (for BPE$_{15}$-LiTFSI$_1$ and BPE$_{15}$—NaTFSI$_1$) and 16 mm (for BPE$_{15}$-KTFSI$_1$) were placed between the alkali metal electrodes. Prior to the measurements, the cells were pre-conditioned at a temperature of 55 °C for 1 h The impedance data were collected in a frequency range from 1 MHz to 100 mHz with an amplitude of 10 mV. Afterwards, direct current polarization was applied with a polarization voltage of ΔV = 50 mV, while the impedance spectra were recorded before and after the polarization, respectively. The transference number T_A^+ was calculated using Eq. (2):

$$T_A^+ = \frac{I_s \, (\Delta V - I_0 \, R_0)}{I_0 \, (\Delta V - I_s \, R_s)} \tag{2}$$

where I_0 and I_s represent the initial and steady-state current, respectively, ΔV is the polarization voltage, and R_0 and R_s are the initial and steady-state electrode resistance (R_{CT} and R_{SEI}), respectively. The initial current I_0 can be calculated using Eq. (3):

$$I_0 = \frac{\Delta V}{R_b + R_0} \tag{3}$$

where R_b is the resistance of the polymer electrolyte estimated from the Nyquist plot (EIS before polarization). The initial current I_0, which can be calculated according to Eq. (3), is equal to the experimental value, which can be derived from the polarization plot.

2.4.4.2. Pulsed field gradient NMR (PFG NMR).
The temperature-dependent ^{7}Li and ^{19}F solid-state pulsed-field gradient NMR experiments were performed on a Bruker Avance spectrometer at a magnetic field of 7.05 T and a maximum gradient strength of 30 T/m. The data was acquired in a temperature range from 29 to 73 °C using a stimulated-echo pulse sequence. For the ^{19}F PFG experiments, a gradient duration of 1 ms and a diffusion time of 200 ms were used. The gradient duration and diffusion time for the ^{7}Li PFG experiments were set to 4 and 200 ms, respectively. The recycle delay was set to 3.5 – 8 s for the ^{19}F experiments and to 1.6 – 2 s for ^{7}Li experiments and was always well above 5 times T_1.

2.5. Electrode preparation and cell assembly

2.5.1. Electrode preparation

The Prussian blue analogues (PBA) A$_2$Fe[Fe(CN)$_6$] of sodium and potassium (A=Na, K) were used as active materials in the preparation positive electrodes. Na$_2$Fe[Fe(CN)$_6$] (NaFF) and K$_2$Fe[Fe(CN)$_6$] (KFF) are also commonly known as Prussian whites (PW). NaFF positive electrodes were prepared by mixing 0.180 g of Na$_{1.88}$Fe[Fe(CN)$_6$] × 0·7H$_2$O (NaFF, Altris AB, Sweden), 0.090 g of carbon black (SuperC, Imerys Graphite & Carbon, Switzerland), PVdF (HSV900, Arkema), 0.030 g of PEO (average M_v = 100,000 g mol^{-1}, Sigma-Aldrich), and 0.013 g of NaTFSI (52.4: 26.2: 8.8: 8.8: 3.8 ratio by mass, wt.%) in 2 mL of N-methyl-2-pyrrolidone (99.5 wt.%, Sigma-Aldrich). The container was then transferred to a planetary mixer (Thinky, ARV 310-P) and the slurry further mixed at 2000 rpm for 1 h The resulting homogeneous slurry was cast onto a conductive carbon-coated aluminum foil (MTI Corporation, USA) using a doctor blade with a gap of 150 μm. Then, the electrode coating was dried in a climate chamber at 60 °C overnight, and the electrode sheet was densified to a thickness of ~40 μm and cut into discs with a diameter of 16 mm. The electrode discs with a mass loading of ~1 mg cm^{-2} were then dried at 110 and 170 °C, respectively, for 12 h under vacuum (10^{-3} mbar) and transferred in an Ar-filled glovebox without further exposure to air or moisture. KFF positive electrodes were prepared according to the same procedure described above, i.e. a slurry comprising 0.180 g of KFF, 0.090 g of carbon black, PVdF, 0.030 g of PEO, and 0.014 g of KTFSI (52.3: 26.2: 8.7: 8.7: 4.1 ratio by mass, wt.%) was prepared and coated on C-coated Al foil. The thus prepared electrodes were dried at 110 °C for 12 h under vacuum (10^{-3} mbar) prior to use and subsequently stored in an Ar-filled glovebox.

2.5.2. Symmetrical cell assembly

Symmetrical A/SPE/A (A = Li, Na, K) coin-type cells (CR2032-type) were assembled for plating and stripping experiments. SPEs BPE$_{15}$-ATFSI$_1$ with a molar ratio of EO:A = 15:1 were prepared as described in Section 2.4. The electrolyte discs with a thickness of ~100 μm and a diameter of 8 mm (for BPE$_{15}$-LiTFSI$_1$ and BPE$_{15}$—NaTFSI$_1$) and 16 mm (for BPE$_{15}$-KTFSI$_1$) were placed between the alkali metal electrodes. Prior to the measurements, the cells were pre-conditioned at a temperature of 55 °C for 2 h

2.5.3. Full cell assembly

Coin cells were assembled using a Na-metal negative electrode (99.8 wt.%, Alfa Aesar), and a NaFF-based positive electrode and respective electrolyte. For the Na-cell with organic liquid electrolyte, glass fiber separators (Whatman GF/B) were dried at 110 °C for 12 h under vacuum (10^{-3} mbar), and one layer of the separator was soaked with 150 μL of an electrolyte comprising a 0.5 M NaPF$_6$ (98 wt.%, Sigma-Aldrich) solution in a mixture of ethylene carbonate (EC) (99 wt.%, Sigma-Aldrich)

and diethyl carbonate (DEC) ($\geq$99 wt.%, Sigma-Aldrich) (1:1 ratio by volume). For the cells with SPEs, $(BPE)_{15}$—$NaTFSI_1$ with a molar ratio of EO:Na = 15:1 was prepared as described in Section 2.4. The electrolyte discs with a thickness of ~100 μm and a diameter of 16 mm were placed between the positive electrodes dried at 110 and 170 °C, respectively, and negative sodium metal electrodes. In the case of the K-battery, K/$SPE/K_{1.90}Fe[Fe(CN)_6]$ cell comprising a K-metal negative electrode (98 wt.% stored in mineral oil, Sigma-Aldrich), a KFF-based positive electrode, a BPE_{15}-$KTFSI_1$ SPE with molar ratio of EO:K = 15:1 was assembled according to the same sequence of procedures described above. Prior to galvanostatic cycling, the LE-cell and SPE-cells were preconditioned at temperatures of 25 and 55 °C for 2 and 20 h, respectively.

2.6. Electrochemical tests

2.6.1. Alkali metals plating and stripping experiments in symmetrical cells

Alkali metal plating and stripping experiments were performed on a VMP-300 potentiostat (BioLogic Science Instruments) at a temperature of 55 °C. For the experiments, the current density (j, where $j = I/A$) was increased stepwise every 10 cycles. Each cycle comprised plating and stripping (for 1 h each, for 20 h in total) at current densities j of 0.01, 0.02, 0.05 and 0.01 mA cm^{-2}.

2.6.2. Galvanostatic cycling

Galvanostatic cycling tests of Na/BPE_{15}—$NaTFSI_1$/NaFF and K/BPE_{15}-$KTFSI_1$/KFF cells were conducted on a VMP-300 potentiostat (BioLogic Science Instruments) at a temperature of 55 °C. The Na-cell was cycled at the cycling rate C/15 (1C = 150 mAh g^{-1} with respect to the theoretical capacity of $Na_{1.88}Fe[Fe(CN)_6] \times 0 \cdot 7H_2O$), and the voltage cut-offs were 2.0 and 4.0 V vs Na^+/Na. For galvanostatic cycling of K/BPE_{15}-$KTFSI_1$/KFF cell, the cycling rate was C/15 (1C = 141 mAh g^{-1} with respect to the theoretical capacity of $K_{1.90}Fe[Fe(CN)_6] \times 1 \cdot 0H_2O$), and the voltage cut-offs were 2.5 and 4.3 V vs K^+/K. In both cases, a constant potential (CP) step for 1 h was added after each charge/discharge sequence. The data was exported to .txt-files using the EC-Lab software (V11.27) and further processed using the in-house developed «bat2dat» R package available on github [27].

3. Results and discussion

3.1. Solid polymer electrolytes

Prior to the preparation of the SPEs, the poly(vinyl benzyl methoxy poly(ethylene oxide) ether)-*block*-polystyrene block copolymer, i.e., PVBmPEO-*b*-PS or BP, was prepared as previously reported (Scheme 1) [22]. The average length of the mPEO side chain with a molar mass of 2.000 g mol^{-1} was determined using ^{1}H-NMR spectroscopy and calculated to an average number of ~48 EO units per side chain. In addition, the blocks of BP were matched to a weight ratio of around 50:50 to target self-standing films. Overall, the block copolymer with a molar mass (M_n) of 38.300 g mol^{-1} (as determined by size exclusion chromatography, SEC, and ^{1}H-NMR) was obtained [22].

The synthesized block copolymer BP was further used to prepare the corresponding block copolymer electrolyte (BPE) compositions using TFSI$^-$-based ion-conducting salts with different cations of alkali metals, namely Li, Na, and K, with varying the molar ratio of EO:A (20:1, 15:1, 10:1). Herein, the impact of the cation size of the ion-conducting salt and its concentration on thermal, rheological, and electrochemical characteristics of the BPE_x-$ATFSI_y$ (where the ratio of *x:y* corresponds to EO:ATFSI molar ratio) was evaluated for their suitability as SPEs in battery applications.

3.2. Thermal and rheological characterization

In general, a lower glass transition temperature (T_g) can be seen as an indicator of higher ionic conductivity in PEO-based electrolytes since it

expresses more mobile segmental chain motion, which significantly assists ion transport. Furthermore, to achieve improved ionic conductivity, crystalline phases should be absent because ion transport principally occurs in the amorphous phase[28–30]. Therefore, the investigation of thermal properties of potential polymer electrolytes (PEs) is highly relevant for the further study of their ionic conductivity. Herein, thermal properties of BPE-ATFSI (A = Li, Na or K) with different molar ratio of EO:A (20:1, 15:1, 10:1) were investigated by DSC (Fig. 1). Notably, all investigated SPEs featured two distinct T_g's, one in the temperature range from −56.5 to −41.3 °C and one around 100 °C (summary given in Table 1), corresponding to the PEO phase and the PS phase, respectively. As shown previously, with a BPE-LiTFSI electrolyte, a lamellar microphase-separated morphology is obtained, allowing both ion transport properties and mechanical strength (enabled by PEO and PS blocks, respectively) [22]. Hence, BPE-ATFSI SPEs can benefit from structural integrity that would potentially prevent a short circuit, inhibiting metallic dendrite growth [17,18,31]. Structural integrity, therefore, is a highly desirable property to have in any separating layer that contacts a metallic anode.

The T_g values of the PS phase in all investigated compositions were detected in the temperature range of ~99-103 °C (Table 1), showing no significant shift and thus, indicating the absence of neither cation size nor salt concentration influence on the PS phase formation. However, the BPE-ATFSI SPEs showed a notable shift of the PEO phase T_gs, depending on A^+ type as well as EO:A molar ratio.

The T_g increased with an increase of ion-conducting salt concentration among the same cation type (Fig. 1d, given in Table 1). This tendency can be explained by the phenomena of quasi-ionic cross-linking [20,22,33–35], manifested by physical interactions between A^+ and PEO side chains that originates from the coordination of cations. As the number of cationic species in BPEs increased, a larger degree of physical cross-links restricting segmental motion of PEO chains was present, therefore, increasing the T_gs. Furthermore, the cation size seemed to impact the BPE-ATFSI thermal properties, shifting the T_g values towards lower temperatures with larger A^+ size (Fig. 1d, Table 1). Assuming a coordination number of 6 for all three cations, the Shannon's effective ionic radius increases in the row Li$^+$ < Na$^+$ < K^+ (0.76, 1.02, 1.38 Å, [36]). Since crystallographic studies on Li-, Na- and K-PEO complexes have suggested weaker coordination (larger A-EO bond lengths) to bigger cations, and higher coordination number, when replacing Li$^+$ and Na$^+$ by larger cations like K^+ or Rb$^+$ [24,25,37], the given values of effective ionic radii for Li$^+$, Na$^+$, K^+ can be merely considered as the first approximation. Nevertheless, larger cations exhibit lower charge density and tend to form less interchain links, i.e., quasi-ionic cross-linking, and therefore could feature faster chain dynamics. This could potentially benefit faster cation transport in Na- and K-ion conductors, compared to Li-SPEs [23–26].

It is noteworthy that addition of ATFSI not only influences the T_g of resulting BPEs, but also significantly impacts their crystallinity. For comparison, T_m of the pristine BP was determined to be 47.3 °C and had a melting enthalpy (ΔH_m) of 52.9 $J\,g^{-1}$ (Figure S1). However, BPE_{20}-$ATFSI_1$ already demonstrated a decrease of the melting temperatures (T_ms) and ΔH_ms (Fig. 1a), which indicates the crystallinity has been suppressed due to the presence of bulky TFSI$^-$ anions hindering chain alignment [38]. With increasing salt concentration (BPE_{15}-$ATFSI_1$, BPE_{10}-$ATFSI_1$) fully amorphous materials were obtained, indicated by the absence of any endothermic peaks (Fig. 1b,c) and two T_gs for both the PEO and PS phases. Interestingly, in PEO-LiTFSI systems (no block copolymer), the absence of crystalline domains is well-known as the 'crystallinity gap' in a compositional range between 6:1 < EO:Li < 12:1 [41]. In contrast, PEO-based samples containing Na- or KTFSI were found to remain semi-crystalline over a wide range of molar ratios (1:1 < EO:Na < 64:1[40] and 1.5:1 < EO:K < 60:1[21,39], respectively). As highlighted above, the presence of crystalline phases may result in inhibited segmental motion of polymeric chains, thus potentially slowing down ion transport. Therefore, at temperatures below T_m BPE_{15}- and
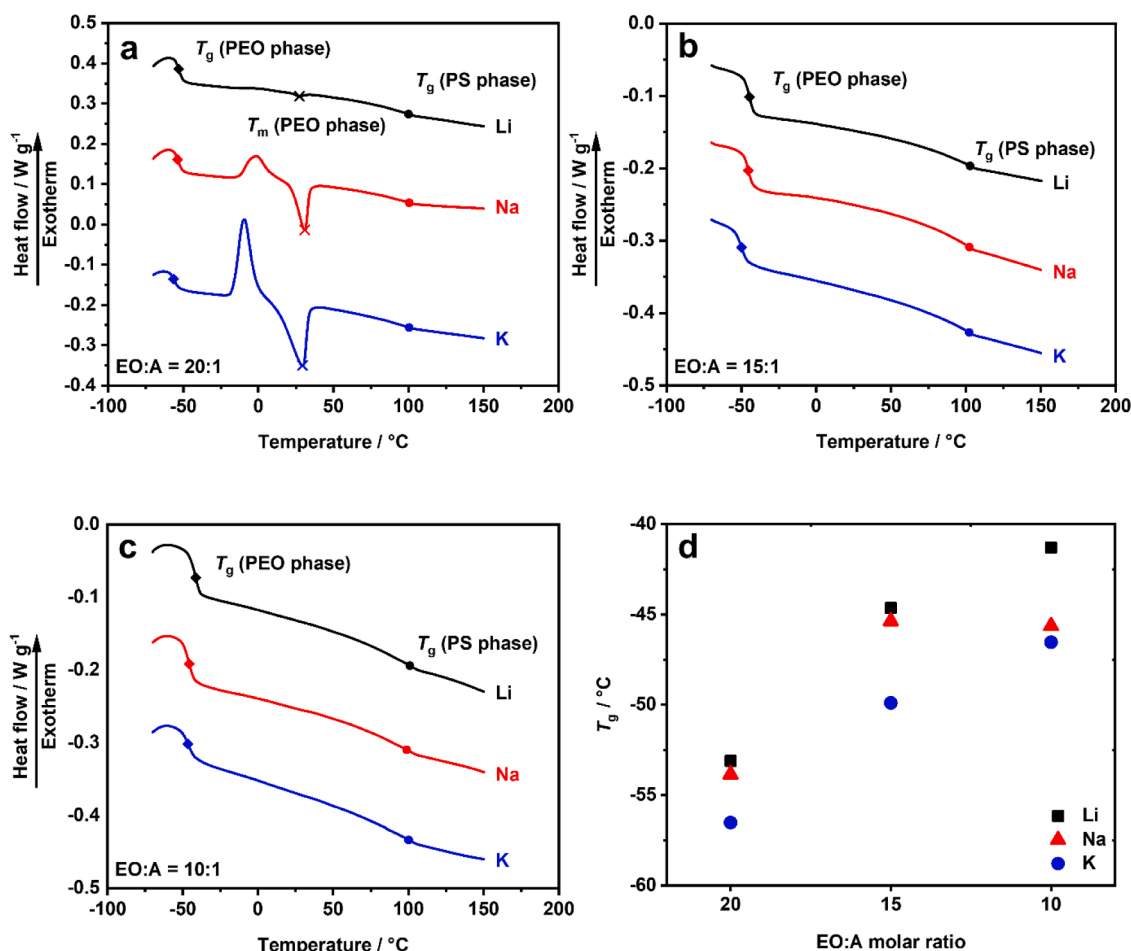
Fig. 1. DSC thermograms of BPE-ATFSI (A = Li, Na or K) with different molar ratios of EO:A (a) 20:1 (b) 15:1 (c) 10:1 recorded at a heating rate of 10 K min^{-1}. (d) Dependency of T_g (PEO phase) on the EO:A molar ratio in BPE-ATFSI SPEs.

Table 1
Thermal characterization (T_g, T_m, ΔH_m, and crystallinity) of the BPE-ATFSI (A = Li, Na or K) with different molar ratio of EO:A.

EO:A, molar ratio	Cation, A^+	T_g (PEO phase), °C	T_g (PS phase), °C	T_m (PEO phase), °C	ΔH_m (PEO phase), J g^{-1}	Crystallinity * (PEO phase), %
20:1	Li	−53.1	100.1	27.3	0.2	0.2
	Na	−53.8	100.5	30.9	5.4	5.5
	K	−56.5	100.6	29.6	11.9	12.1
15:1	Li	−44.6	102.7	–	–	–
	Na	−45.4	102.4			
	K	−49.9	102.2			
10:1	Li	−41.3	101.0	–	–	–
	Na	−45.6	98.9			
	K	−46.5	100.1			

* Calculated relative to theoretical ΔH_m of PEO, 196.4 J g^{-1} [32], divided by two, 98.2 J g^{-1} (since BPE blocks were matched to ∼ 50:50 wt ratio).

BPE$_{10}$ATFSI$_1$ (A = Na, K) might be advantageous in terms of ionic conductivity over the corresponding polymer electrolytes based solely on PEO.

For BPE$_{20}$-ATFSI$_1$ SPEs, a slight increase of T_m was observed for larger cations. Moreover, their influence was reflected in an increasing melting enthalpy, i.e., higher degree of crystallinity of the PEO phase. As shown in Table 1, BPE$_{20}$-LiTFSI$_1$ possessed a negligible crystallinity of 0.2%, while Na- and KTFSI-based SPEs showed larger values of 5.5 and 12.1%, respectively. The reason for this behavior is not entirely clear,

since NaTFSI and KTFSI exhibit lower dissociation energies [23] and weaker cation-anion interactions are generally expected in comparison to LiTFSI. As mentioned above, both the confined environment of the microphase-separated morphology of the polymer film and the chain coordination, which depends on the cation size [37], likely play an important role in the specific coordination environments.

Based on the BPE$_x$-ATFSI$_y$ thermal properties, the largest ionic conductivity is expected for blends employing 15:1 molar ratio of EO:A, as these not only exhibit a completely amorphous state [28], but also have the lowest T_gs among the investigated non-crystalline compositions.

To examine the rheological properties and therefore evaluate the mechanical integrity of the SPEs, small amplitude oscillatory shear (SAOS) measurements were conducted. As shown in Fig. 2, the frequency dependence of the shear storage (G') and loss (G'') moduli of the BPE compositions with the molar ratio of EO:A = 15:1 were measured at ambient and elevated temperatures (25 and 55 °C, respectively). Herein, the shear storage modulus G' quantifies the elastic portion of viscoelastic behavior, while G'' represents its viscous portion [42]. Thus, when sheared, G' > G'' indicates viscoelastic solid-like behavior, whereas G' < G'' expresses viscoelastic liquid-like behavior. Therefore, G' and G'' quantifies the mechanical strength required of SPEs, since they serve a) as separators between cathode and anode in the cell configuration and b) should hinder metallic dendrite growth. Often, mechanical stiffness in PEO-based electrolytes is induced by the polymer's inherent crystallinity [14,43] that restrains chain movement. At the same time, restricted segmental motion results in inhibited ion transport in polymer-based blends [20]. At temperatures above T_m of the PEO phase, the crystalline regions disappear, which results in enhanced
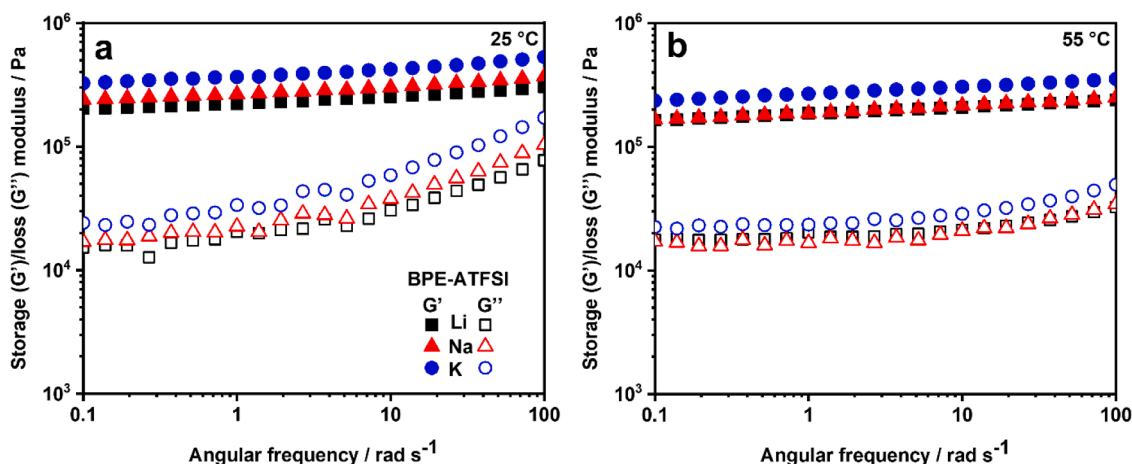
Fig. 2. Dependency of shear storage (G') and loss (G'') moduli on angular frequency of BPE$_{15}$-ATFSI$_1$ (A = Li, Na or K) at (a) 25 °C and (b) 55 °C.

ion mobility at expense of mechanical integrity [21]. To overcome this issue, BPE was designed to feature a decoupling of the segmental motion from charge transport by microphase-separation. Here, the PS block possesses a high mechanical stiffness (G', G'' of ~1 GPa)[44], which is relevant for the suppression of metallic dendrite growth [17,18,45].

At ambient temperature (Fig. 2a), G' > G'' was observed for all examined compositions, indicating their dominating solid-like behavior [42] in the investigated frequency range (from 0.1 to 100 rad s^{-1}). The storage moduli of the BPE compositions were found in the range of 2.0–5.3 × 10^5 Pa, showing a weak dependence on the frequency. In addition, the moduli for the SPEs containing LiTFSI and NaTFSI were similar, while BPE-KTFSI exhibited slightly higher values. This observation was somewhat unexpected, since the SPE with KTFSI possessed the lowest T_g of the PEO phase (Table 1). Since the batteries employing SPEs typically operate in a higher temperature range, it is relevant to examine the mechanical stability of the samples at an elevated temperature (here 55 °C). As presented in Fig. 2b, the block copolymer-based compositions maintained G' > G'', and only slightly lower moduli, indicating a negligible loss of mechanical stability at 55 °C due to the presence of the rigid PS block [22,46]. For comparison, a pure PEO-based PE with a close ratio of EO:A (PEO$_{16}$-KTFSI$_1$) reported in our previous study [21], displayed G' of almost one order of magnitude lower than BPE$_{15}$-KTFSI$_1$ at 25 °C. Further, at 55 °C the PEO$_{16}$-KTFSI$_1$ showed a drastic decrease of both storage and loss moduli that is typically observed for semi-crystalline compositions above their T_m due to the melting of the rigid crystalline phase [47]. Moreover, at low frequencies PEO-based samples manifested liquid-like behavior (G' < G'') [48], contrary to BPE-ATFSI, maintaining the mechanical integrity at given conditions due to the stiffness of the PS phase with a high T_g of around 100 °C.

Overall, the thermal and rheological characterization of BPE-ATFSI demonstrated the advantage of PS block copolymerization over the pure PEO polymer chain: the enhancement of mechanical strength due to the formation of a microphase separated PS phase that does not disturb ion transport enabled by PEO [22].

3.3. Ion transport

To evaluate the ionic conductivities (σ) in BPE-ATFSI (molar ratio of EO:A = 20:1, 15:1 or 10:1) employing various conducting ions (Li$^+$, Na$^+$ or K^+), EIS was carried out in a temperature range of 5–85 °C with 10 °C steps (**Figure S2**). As already highlighted in the discussion of thermal properties (see Section 3.2), the largest σ values were expected for the amorphous BPE$_{15}$-ATFSI$_1$ due to their lower T_g (PEO phase) values. As seen in Fig. 3, this expectation was confirmed, as the highest ionic conductivities were observed for these compositions regardless of the
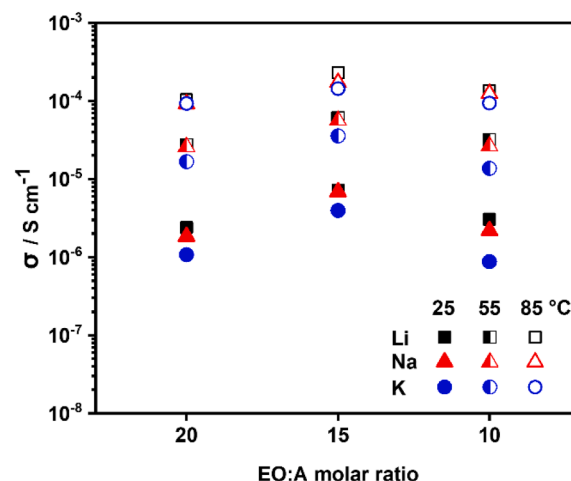

Fig. 3. Dependency of ionic conductivity (derived from EIS in the frequency range from 1 MHz to 500 mHz) in BPE$_{15}$-ATFSI$_1$ (A = Li, Na or K) on the EO:A molar ratio at 25, 55 and 85 °C.

employed cation. The BPE$_{15}$-LiTFSI$_1$ sample showed the highest ionic conductivity of 7.20 × 10^{-6} S cm^{-1} at a temperature of 25 °C. For comparison, a slightly lower value (~3 × 10^{-6} S cm^{-1}) was reported for semi-crystalline PEO$_{15}$-LiTFSI$_1$ at the same temperature [49]. The higher ionic conductivity at ambient temperature in BP-based electrolytes can be associated with its amorphous state enabled by the sophisticated architecture, in contrast to the semi-crystalline nature of pure PEO-based samples. In general, a fully amorphous nature above T_g facilitates enhanced dynamic segmental motion of the polymer chain and assists ion hopping motion [50,51]. Higher values of ionic conductivity however were reported for PEO$_{15}$-LiTFSI$_1$ at temperatures above its T_m, where the adverse impact of crystalline regions on ionic transport disappears, but at the cost of a loss of mechanical integrity. In comparison to PEs based solely on PEO, block copolymers feature lower PEO domain fractions due to the additional PS phase. Therefore, at higher temperatures they possess relatively modest ionic conductivities, while the mechanical stability is significantly improved [22].

A peak ionic conductivity was found at EO:A molar ratio of 15:1 (e.g. 7.2 × 10^{-6} vs. 2.4 × 10^{-6} and 3.1 × 10^{-6} S cm^{-1}, for EO:Li = 15:1, 20:1 and 10:1, respectively, at 25 °C), which supports thermal characterization. For the compositions with EO:A = 20:1, suppressed ion transport was probably caused by two effects: I) their semi-crystalline nature and II) a lower concentration of charge carriers, i.e., conducting ions. Surpassing T_m of these blends (~30 °C, given in Table 1), a significant

increase of σ was observed (**Figure S2b**) as a result of the dissolution of any remaining crystalline regions [20,28]. However, even above T_ms of the BPE$_{20}$-ATFSI$_1$, the ionic conductivity of the SPEs with EO:A = 15:1 could not be reached (4.4–7.1 × 10^{-6} vs. 1.0–1.8 × 10^{-5} S cm^{-1}, respectively, at 35 °C, **Figure S2b,c**), probably due to the lower ATFSI concentration (i.e. charge carriers) in 20:1 electrolyte formulations. Conversely, the SPEs with EO:A = 10:1 possessed the largest content of charge carriers, but still restrained ion transport was observed (Fig. 3) compared to the 15:1 SPEs. This can be explained by the higher T_g (PEO phase) of BPE$_{10}$-ATFSI$_1$ and probably more quasi-ionic cross-linking as a result of the higher cation concentration [20,35,52]. Consequently, the BPE$_{15}$-ATFSI$_1$ samples were chosen for further electrochemical tests as these compositions not only featured the highest ionic conductivity but also provided sufficient mechanical stiffness.

As discussed for the thermal characterization (Section 3.2), the size of A^+ in BPE-ATFSI SPEs affected their T_g (PEO phase) values, manifesting a decrease towards potassium-based electrolytes (Fig. 1d, Table 1). Based on this, we assume that cations with a smaller ionic radius (Li$^+$) are more tightly bound to the PEO segments as larger cations (Na$^+$ and K^+) [24,25], which could lead to a faster cation transport for Na$^+$ and K^+ resulting in higher cation transference numbers [23]. Therefore, the highest (cat)ion transport was expected for KTFSI-based compositions. Contrary to this assumption, a slight decline of the ionic conductivity was observed with increasing the size of A^+ (Fig. 3). However, the ionic conductivity in dual-conducting SPEs is generally a complex contribution of both anion and cation mobilities, as well as associated, charged ion pairs such as [A$_2$X]$^+$ or [AX$_2$]$^-$. To evaluate the contribution of Li$^+$, Na$^+$ or K^+ to the total ionic conductivity,

measurements of the actual A^+ transference number are required.

3.4. Transference number measurements

3.4.1. Bruce-Vincent method

We attempted to measure transference numbers T_A^+ of BPE$_{15}$-ATFSI$_1$ SPEs using the commonly employed Bruce-Vincent method [53], i.e., combination of potentiostatic polarization and EIS in symmetrical A/SPE/A cells (summary given in **Table S1**, Fig. 4). As we used the SPE films with different area for this experiment (see **Experimental section**), dependency of the current density (j, where $j = I/A$) on time and area specific resistance (ASR, Ohm cm^2) derived from EIS spectra were plotted in Fig. 4 for better comparability.

First, T_{Li}^+ of BPE$_{15}$-LiTFSI$_1$ was measured at elevated temperature of 55 °C and ΔV = 50 mV (Fig. 4a). A constant dc bias potential in this study was set to 50 mV, as it should be low enough to obtain linear response of the system, yet high enough to receive reasonable current values considering the larger initial resistances R_0 of Na- and K-cells. As can be seen in the chronoamperometry, the Li/BPE$_{15}$-LiTFSI$_1$/Li cell reached approximately a steady state after ~0.5 h with a current change from an initial value I_0 of 0.074 mA (j = 0.147 mA cm^{-2}) to a steady-state value I_s of 0.027 mA (j = 0.054 mA cm^{-2}), resulting in I_s/I_0 ratio of 0.36 (**Table S1**). Moreover, to guarantee accuracy of the measurement, the theoretical I_0 was calculated to 0.08 mA (through Ohm's law, Eq. (3)), being in line with the experimental value. After polarization, the cell exhibited a slightly larger overall resistance than initial value (**Table S1**, ΔR = 15 Ohm). According to Eq. (2), T_{Li}^+ of BPE$_{15}$-LiTFSI$_1$ was calculated to be 0.13, which is in agreement with our previously
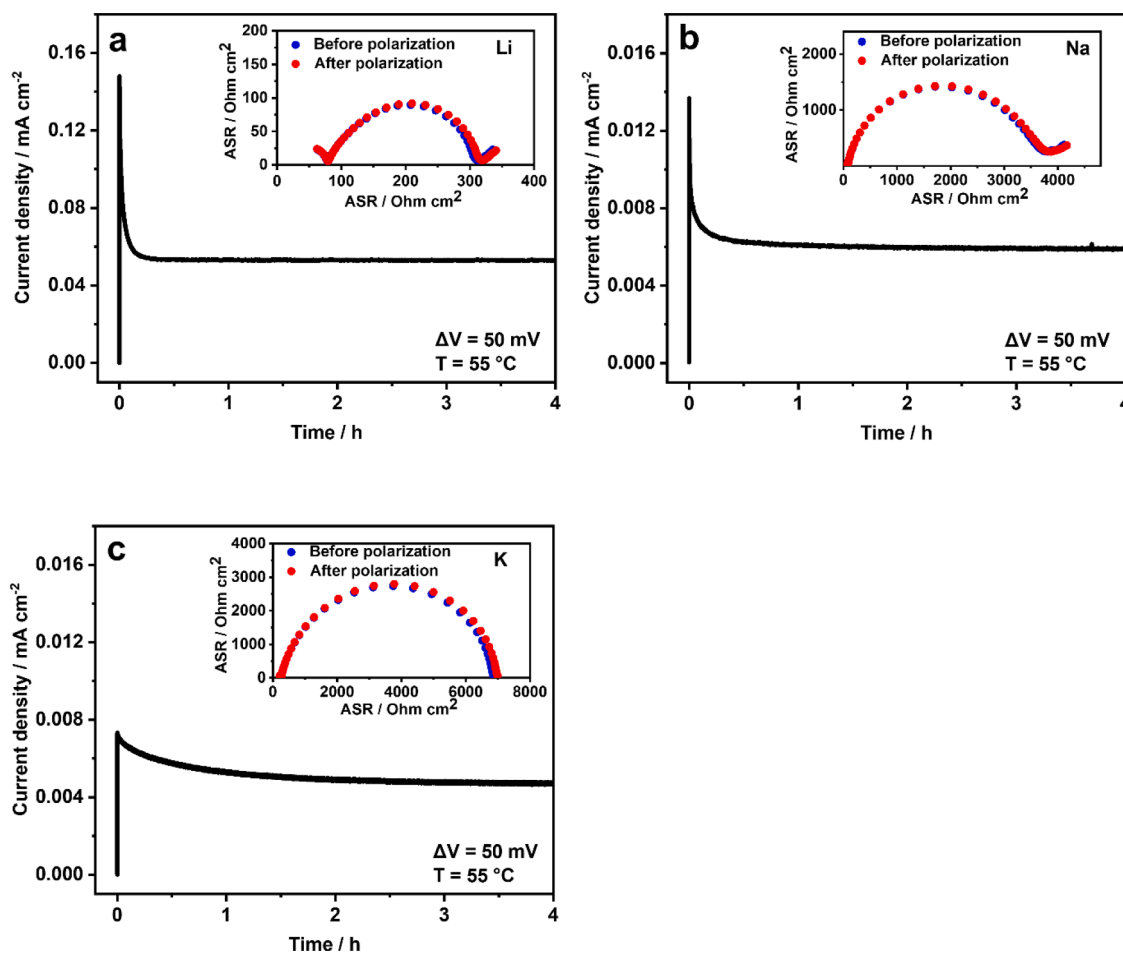

Fig. 4. Chronoamperometry and area specific resistance (ASR) derived from EIS spectra (before and after potentiostatic polarization, recorded in the frequency range from 1 MHz to 100 mHz) of A/BPE$_{15}$-ATFSI$_1$/A cells where A = (a) Li, (b) Na, (c) K, at ΔV of 50 mV and temperature of 55 °C.

reported result [22]. However, we encountered difficulties in determining T_{Na}^+ and T_K^+ using the Bruce-Vincent technique. As compared to the Li-cell, both Na/SPE/Na and K/SPE/K showed one order of magnitude larger initial ASR (Fig. 4b,c) as well as larger R change after polarization (ΔR = 129 and 61 Ohm for Na and K-cells, respectively, Table S1). Subsequently, for Na/K-cells smaller I and j values were observed. However, for both cells I_0 values were in line with the theoretically calculated I_0 (Table S1). Furthermore, the ratio of steady-state to initial current increased from Li- to Na- and K-cell (I_s/I_0 = 0.36, 0.43 and 0.60, respectively), indicating a smaller current decay in the post-Li systems. In a setup with non-blocking, yet inert, electrodes, an increase in the I_s/I_0 ratio could be interpreted as a sign of higher ionic mobility. However, sodium and potassium electrodes are well known for their high reactivity towards electrolyte components [1,54] and thus may also exhibit a leaking current from recurrent degradation reactions. On the other hand, the impedance measurements before and after polarization suggest that, although the interfacial resistance is considerably larger in Na and K cells, the cell impedance did not change significantly. Considering the high SEI resistance, however, the calculated transference numbers T_{Na}^+ and T_K^+ were −0.03 and 0.02, respectively. Although, the Bruce-Vincent method is the most commonly used method to determine the transference numbers, its shortcomings are well described in literature [55].

In addition, there appeared to be more problems with the potentiostatic polarization in symmetrical Na/SPE/Na and K/SPE/K cells, compared to setups comprising Li-metal electrodes. As stated above, the interfacial resistance at the Na- or K-electrolyte interface is substantially larger, by one order of magnitude. With the transport across the electrode-electrolyte interface being a determining factor, no meaningful parameters could be obtained. Furthermore, the variance in the impedance and polarization experiments increases tremendously, making it even more challenging to extract reliable parameters from this approach. It is worth noting that similar observations have been reported in literature [56,57], indicating that the Bruce-Vincent method is difficult to adapt to post-Li systems.

3.4.2. Pulsed-field gradient nuclear magnetic spectroscopy (PFG NMR)

Given the shortcomings of the Bruce-Vincent method discussed above, we attempted to evaluate $T_{Na/K}^+$ using a non-electrochemical method. As the alkali metal cations herein possess NMR-active nuclei (^{7}Li, ^{23}Na, ^{39}K), their self-diffusion coefficients (D_A^+) can be determined by pulsed-field gradient (PFG) NMR. Likewise, the anion diffusion coefficient (D_{TFSI}^-) can be obtained from the PFG NMR of ^{19}F active nuclei in the TFSI$^-$ anion. Furthermore, the cation transference number T_A^+ can be calculated from cation and anion diffusion coefficients according to Eq. (4):

$$T_{A^+} = \frac{D_{A^+}}{D_{A^+} + D_{TFSI^-}} \tag{4}$$

Notably, Eq. (4) can be used assuming that A^+ and TFSI$^-$ are the only mobile species that move in polymer matrix independently. The PFG NMR study was performed on BPE$_{15}$-LiTFSI$_1$, BPE$_{15}$—NaTFSI$_1$, and BPE$_{15}$-KTFSI$_1$ samples. Firstly, the dependence of echo intensity on the gradient field strength g in the temperature range from 29 to 73 °C in steps of 11 °C was measured for ^{7}Li and ^{19}F species (Figure S3a,b, respectively) in BPE$_{15}$-LiTFSI$_1$.

The dependence of the echo intensity on the gradient field strength g can be described by a Gaussian function [58], and it decays proportional to $\exp\left(-(\delta \gamma g)^2 \times (\Delta - \frac{\delta}{3}) \times D\right)$, where δ is the gradient pulse duration, γ the magnetogyric ratio of the observed nuclei, Δ the diffusion time, and D the temperature-dependent diffusion coefficient. In general, a faster diffusion results in a faster decay of the response signal to zero. As expected, the diffusion of both Li$^+$ and TFSI$^-$ ions is enhanced with increasing temperature (Figure S3a,b), which is related to more mobile segmental motion of polymer chains at elevated temperatures.

The temperature dependence of D well above T_g can be described by an Arrhenius behavior according to Eq. (5):

$$D = D_0 \times \exp\left(\frac{-E_a}{k_B \times T}\right) \tag{5}$$

where D_0 is the prefactor, E_a the activation energy, k_B the Boltzmann constant, and T the absolute temperature. It is known that the ionic conductivity in amorphous polymers is coupled to segmental motions, thus relating ion transport to free volume theory. The temperature dependence of the ionic conductivity in amorphous polymers typically displays Vogel-Fulcher-Tammann (VFT) (Eq. (6)) rather than the conventional Arrhenius behavior.

$$D = D_0 \times \exp\left(\frac{-E_a}{k_B \times (T - T_0)}\right) \tag{6}$$

where T_0 is «Vogel temperature», typically ca. 50 K below T_g [20].

However, the behavior can be different in polymer host media with a rigid framework and tortuosity [20], and it has not yet been investigated in detail for BPE-based electrolytes. Herein, the temperature-dependent self-diffusion coefficients were extracted for ^{7}Li and ^{19}F, and are shown in Figure S3c,d, respectively. Noteworthy, dependence of the extracted D_{Li}^+ and D_{TFSI} on temperature seemed to display Arrhenius behavior (Figure S3c,d), while the temperature-dependent ionic conductivity (derived from EIS) in BPE$_{15}$-LiTFSI$_1$ (Figure S2c) rather followed VFT behavior. However, for PFG NMR measurements, only a limited temperature range was investigated (from 29 to 73 °C) that might be not enough to reveal VFT behavior. From Figure S3c, the ^{7}Li activation energy E_a was calculated to 0.52±0.02 eV (summary given in Table 2). A similar value of E_a was found for ^{19}F (0.51±0.01 eV, Figure S3d). However, faster diffusion of approximately one magnitude was observed for ^{19}F. With known parameters of D_0 and E_a, one can calculate the diffusion coefficients at any temperature within the measurement range between two phase transitions, using the Arrhenius temperature dependence. Therefore, D of both Li$^+$ and TFSI$^-$ species in BPE$_{15}$-LiTFSI$_1$ were calculated at ambient (25 °C) and elevated (55 °C) temperatures (Table 2). In the next step, for the BPE$_{15}$-LiTFSI$_1$ system the transference numbers, i.e., T_{Li}^+, at 25 and 55 °C were calculated to 0.183 and 0.185, respectively. The obtained data correlates well with the value of T_{Li}^+ found for BPE$_{15}$-LiTFSI$_1$ through Bruce-Vincent method (0.13, see Table S1), thus indicating consistency across the methods for T_{Li}^+ determination.

Furthermore, we conducted PFG NMR measurements to determine the dependence of echo intensity on the gradient field strength g for ^{23}Na in BPE$_{15}$-NaTFSI$_1$. Unfortunately, our attempts to evaluate the Na$^+$ diffusion were not successful due to very short spin-spin and spin-lattice relaxation times of ^{23}Na nuclei as a result of strong nuclear quadrupole coupling. For ^{39}K, the measurement was not possible because of the small resonance frequency of this nucleus. Nonetheless, PFG NMR was conducted on the ^{19}F nucleus (that have no quadrupolar coupling) in the BPE$_{15}$—NaTFSI$_1$ and BPE$_{15}$-KTFSI$_1$ samples (Figure S4a,b). Compared to the Li-sample, an increased activation energy E_a of 0.55±0.02 eV and

Table 2

Diffusion coefficients (D) and transference numbers (T_A^+) at 25 and 55 °C, calculated from PFG NMR measurements for BPE$_{15}$-ATFSI$_1$ (A = Li, Na, K).

BPE$_{15}$-ATFSI$_1$	Nuclei	E_a, eV	D at 25 °C, m^2 s^{-1}	T_A^+ at 25 °C	D at 55 °C, m^2 s^{-1}	T_A^+ at 55 °C
BPE$_{15}$-LiTFSI$_1$	^{7}Li	0.52 ± 0.02	1.13 × 10^{-13}	0.183	7.83 × 10^{-13}	0.185
	^{19}F	0.51 ± 0.01	5.03 × 10^{-13}		3.18 × 10^{-12}	
BPE$_{15}$-NaTFSI$_1$	^{19}F	0.55 ± 0.02	3.66 × 10^{-13}	–	2.61 × 10^{-12}	–
BPE$_{15}$-KTFSI$_1$	^{19}F	0.55 ± 0.02	3.27 × 10^{-13}	–	2.34 × 10^{-12}	–

reduced diffusion coefficients were obtained for ^{19}F in BPE_{15}—$NaTFSI_1$, revealing its lower anion diffusivity (**Figure S4c**, Table 2). The same E_a value, yet even slightly lower values for D, were found for ^{19}F nucleus in BPE_{15}-$KTFSI_1$, indicating even lower TFSI$^-$ mobility (**Figure S4d**, Table 2). Taking into account that the ionic conductivity of BPE_{15}-$LiTFSI_1$ and BPE_{15}—$NaTFSI_1$ at 25 °C is nearly the same (7.2×10^{-6} and 6.8×10^{-6} S cm^{-1}, respectively), and the anion diffusion of the TFSI$^-$ in NaTFSI is only 73% of the anion diffusion in LiTFSI, it could be concluded that the self-diffusion of Na$^+$ is in fact higher for Na$^+$ than for Li$^+$. Additionally, for BPE_{15}-$LiTFSI_1$ cationic (σ_{Li+}) and anionic (σ_{TFSI-}) partial conductivities were derived from diffusion coefficients at 25 and 55 °C according to the Nernst-Einstein equation [58] (Eq. (7)):

$$\sigma = \frac{D \times n \times q^2}{k_B \times T} \qquad (7)$$

where n is the concentration of charge carriers and q is the elementary charge. At a temperature of 25 °C, σ_{Li+} and σ_{TFSI-} were calculated to be 4.22×10^{-6} and 1.90×10^{-5} S cm^{-1}, giving a total ionic conductivity of 2.32×10^{-5} S cm^{-1}. At higher temperature of 55 °C, one order of magnitude higher conductivities for Li$^+$ (2.46×10^{-5} S cm^{-1}) and TFSI$^-$ (1.09×10^{-4} S cm^{-1}) were derived, resulting in σ_{total} of 1.34×10^{-4} S cm^{-1}. The conductivities determined by PFG NMR are higher by a factor of 3 than the ones measured using EIS (Section 3.3, 7.20×10^{-6} and 6.04×10^{-5} S cm^{-1} at 25 and 55 °C, respectively). This deviation is most likely related to the limited diffusion length (from 0.4 to 1.5 μm for ^7Li and from 0.9 to 3 μm for ^{19}F) of the PFG NMR experiment in the investigated temperature range (from 29 to 73 °C).

In summary, as presented in Fig. 5, a reduction of the anion mobility along with increasing cation radii in dual-conducting BPE_{15}-$ATFSI_1$ SPEs was clearly observed. Because of technical limitations, PFG NMR was unable to provide a detailed complementary picture of the ion transport in the polymer electrolytes comprising Na- or K-salts. However, the estimations on the anion and cation diffusion coefficients and the resulting ion conductivity point into the direction of increased cation mobility, as the cation size increases. Furthermore, our findings clearly highlight that suitable approaches to reliably and accurately determine T_A^+ values in post-Li systems have yet to be established [55].

3.5. Alkali-Metals plating/stripping in polymer electrolytes

To judge on the interfacial stability of the different BPE_{15}-$ATFSI_1$ (A = Li, Na or K) SPEs against the corresponding alkali metal,

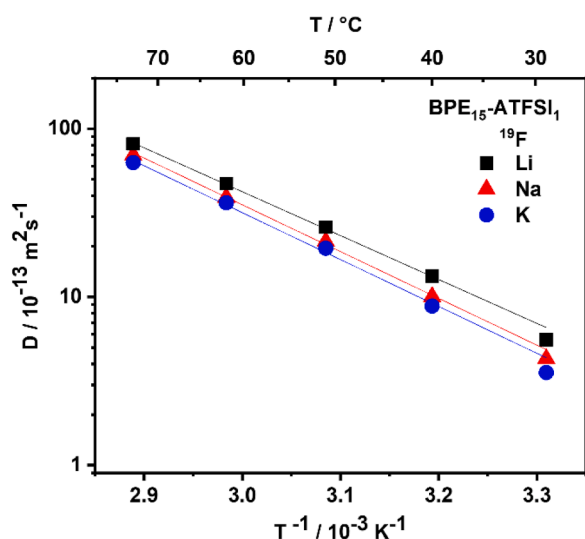**Fig. 5.** Dependence of extracted diffusion coefficients (D) on temperature for ^{19}F PFG NMR in BPE_{15}-$ATFSI_1$ where A = Li, Na, K.

overpotentials originating from plating/stripping in symmetrical A/BPE_{15}-$ATFSI_1$/A cells were determined at current densities (j) of 0.01, 0.02, 0.05 and again 0.01 mA cm^{-2} at 55 °C (each applied for 10 cycles; see details in Experimental section).

As can be seen in Fig. 6, all investigated BPE_{15}-$ATFSI_1$ SPEs enabled a reversible alkali metal deposition at given conditions. However, we observed several differences in the plating/stripping behavior of different A/BPE_{15}-$ATFSI_1$/A systems.

The lithium-based cell developed the lowest overpotentials at given current densities in comparison to both sodium and potassium systems. At an initial j of 0.01 mA cm^{-2}, a maximum overpotential of 10 mV was detected for Li/BPE_{15}-$LiTFSI_1$/Li (Fig. 6a), while sodium- and potassium-cells displayed overpotentials of ~90 and ~80 mV, respectively (Fig. 6b,c). At higher current densities of 0.02 and 0.05 mA cm^{-2}, the overpotentials of Na- and K-cells were almost 10 times larger in comparison to the Li-based one. In general, a higher potential can be attributed to a larger cell resistance, which origins from the resistance of the electrolyte, the SEI as well as the charge-transfer [59]. As seen in the impedance spectra in Fig. 4c, the SEI resistance seemed to play a major role for the overall cell resistance in the Na- and K-cells, while the electrolyte resistance was comparably low. Since a final determination of the transference numbers for the Na- and K-based films however was not possible, it is hard to estimate the actual influence of the ion transport through the polymer electrolytes.

Moreover, at the highest current density j of 0.05 mA cm^{-2} the Li/BPE_{15}-$LiTFSI_1$/Li cell showed an overpotential of 47.5 mV (Fig. 6a), which remained constant ($\Delta V = 0.02$ mV), thus indicating a stable SEI as well as stable deposition behavior. Contrary to this result, Na/BPE_{15}-$NaTFSI_1$/Na displayed a higher initial overpotential of 447 mV, which decreased within following cycles by about 50 mV (Fig. 6b). This behavior was already observed in previous studies and probably corresponds to a refreshed (and thus more ion-conducting) SEI under higher plating/stripping potentials (>100 mV) [1,13]. Slightly lower values of overpotential (~330 mV ± 10 mV) were observed for the K/BPE_{15}-$KTFSI_1$/K system at 0.05 mA cm^{-2} (Fig. 6c). When decreasing the current density to 0.01 mA cm^{-2} again (the last sequence), the cells showed potential values similar to that observed at the initial 10 cycles with 0.01 mA cm^{-2}. During the last sequence, a slight increase of overpotential (up to 10 mV) was observed for Na- and K-cells, while for the lithium-cell the value was constant (see zoomed-in **Figure S5**).

To summarize, these findings showed significantly lower overpotentials for lithium symmetrical cells compared to the corresponding sodium and potassium cells. This generally reflects the high interfacial impedances seen for the post-Li systems in the above data (Fig. 4), which could be ascribed to thicker and/or poorer ion-conducting interface layers. However, we did not observe any short circuit upon metal dendrite growth under the chosen conditions in any of the three systems, indicating the potential of their application in solid-state metal batteries.

3.6. Galvanostatic cycling

Lastly, we investigated the electrochemical properties in long-term galvanostatic cycling experiments in A/BPE_{15}-$ATFSI_1$/cathode cell configuration. As reported in our previous study [22], Li-based full cell employing NMC622 as a cathode, Li-metal as an anode and BPE_{15}-$LiTFSI_1$ as a PE, showed a capacity retention of 63.7% over 100 cycles at a cycling rate of C/10 and a temperature of 60 °C. Remarkably, the cell did not exhibit a rapid capacity fade or voltage noise that are commonly observed for Li-cells employing PEO-based SPEs in combination with NMC622 and associated with metallic dendrite growth [14–16]. Most likely, this can be attributed to the enhanced mechanical stability of the polymer electrolyte, BPE_{15}-$LiTFSI_1$, which inhibits lithium dendrite penetration during charge/discharge processes. Similarly, remarkable stability at high voltages, i.e., a high capacity retention, was reported for the cell comprising a NMC622 cathode, a Li-metal anode and solid-state polycarbonate-based composite electrolyte [60], proving the
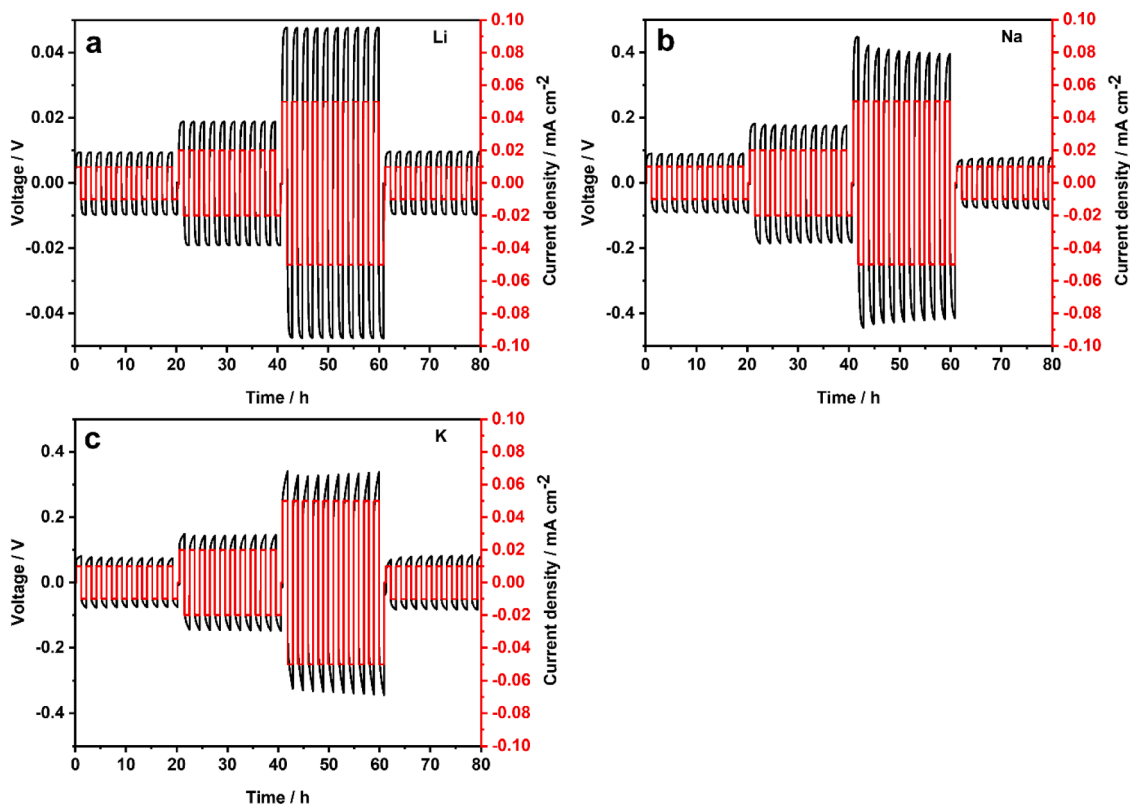
Fig. 6. Plating/stripping experiments in symmetrical A/BPE$_{15}$-ATFSI$_1$/A cells at 55 °C with current densities of 0.01, 0.02, 0.05 and 0.01 mA cm^{-2} for 10 cycles at each current density and 1 h per semi cycle: (a) A = Li, (b) A = Na, (c) A = K.

advantages of SPE applications in alkali metal batteries. Since the focus of this study is on the transition from Li- to Na/K-based batteries, no further full cell tests were performed on lithium-based systems. Instead, the focus was placed on the electrochemical tests for the respective sodium- and potassium-based setups.

As cathode materials, the sodium and potassium-based Prussian whites with the general formula A$_2$Fe[Fe(CN)$_6$] were chosen for their widespread use in post-Li applications and their high cycling stability reported for both liquid and solid-state polymer electrolytes [61–63]. For the Na-cell, a PBA with the chemical composition Na$_{1.88}$Fe[Fe(CN)$_6$] × 0·7H$_2$O (NaFF; theoretical capacity of 150 mAh g^{-1}) was used. For consistency, the corresponding potassium analogue with the general formula K$_{2-x}$Fe[Fe(CN)$_6$]$_{1-y}$ × zH$_2$O (KFF), was synthesized, as described in our previous work[21]. The chemical composition was further determined using a combination of TGA (**Figure S6**) and inductively coupled plasma optical emission spectroscopy (ICP-OES) (**Table S2**) in order to determine the water content and the K:Fe ratio of the compound K$_{2-x}$Fe[Fe(CN)$_6$]$_{1-y}$ × zH$_2$O, respectively. The resulting stoichiometry of the compound was calculated to K$_{1.90}$Fe[Fe(CN)$_6$]$_{0.98}$ (see **Supporting Information**), from which the water content can be determined to z = 1.0, yielding the total stoichiometry K$_{1.90}$Fe[Fe(CN)$_6$]$_{0.98}$ × 1·0H$_2$O that would correspond to a theoretical capacity of ~141 mAh g^{-1}.

Galvanostatic cycling of BPE$_{15}$-Na/KTFSI$_1$ cells was conducted at a cycling rate of C/15 and at an elevated temperature of 55 °C to promote the ionic conductivity in those SPEs (Fig. 3). A voltage window of 2.2–4.0 V vs. Na$^+$/Na was used for Na-cell, while K-cell was cycled with a voltage window of 2.5-4.3 V vs. K$^+$/K (**Figure S7a,b**, respectively). The upper cut-off voltage of 4.3 V vs. Li$^+$/Li was used for the Li/BPE$_{15}$-LiTFSI$_1$/NMC622 cell previously reported [22]. With respect to a common Li-reference in propylene carbonate [64], the upper cut-off voltage would correspond to 4.23 V vs. Li$^+$/Li for the sodium cell and 4.21 V vs. Li$^+$/Li for the potassium cell, respectively. It is useful to bear in mind that PEO degradation was already observed in this potential region

[14–16], although the onset of the degradation potential appears to be strongly dependent on the experimental technique as well as the working electrode material [65].

Capacity retention and corresponding coulombic efficiencies over 100 cycles of the sodium full cell comprising NaFF-based positive electrode, Na-metal negative electrode and BPE$_{15}$—NaTFSI$_1$ polymer electrolyte are shown in Fig. 7a.

In the first cycle of the Na-based cell (Fig. 7a), a discharge capacity of 132.6 mAh g^{-1} was delivered, corresponding to 88% of NaFF theoretical capacity (based on the stochiometry, 150 mAh g^{-1}). The maximum discharge capacity was reached after five cycles with a maximum capacity of 140 mAh g^{-1}. The initial capacity increase is typical for solid-state cells with PEs and can be explained by a conditioning phase in which the electrode-electrolyte contact is gradually improved over time at elevated temperatures [66]. In Fig. 7a, a slight increase of discharge capacity can be seen in the 22nd cycle due to the instrument interruption, which is reflected in a notable drop of CE in the respective cycle. In this study, the Na/BPE$_{15}$-NaTFSI$_1$/NaFF cell retained 73% of its maximum specfic capacity over 100 cycles. Generally, electrochemical performance (in particular, capacity retention) of sodium metal batteries employing NaFF strongly depends on the structural properties of the latter [67–69]. For example, thorough drying at high temperature under vacuum converts the structure from monoclinic to rhombohedral [69] and has a significant impact during cycling on the voltage profiles, the overpotential, as well as the degree of side reactions with water at high potentials (compare **Figure S8a,b**, where NaFF was dried only at 110 °C instead of 170 °C for 12 h under vacuum (10^{-3} mbar) and further cycled at the same conditions). As presented in Fig. 7a, CE notably dropped from the first to the second cycle (from 99 to 97%), which is mainly attributed to the conditioning phase during the initial cycles, as mentioned above. In the following cycles the CE increases again to 98% (up to the 20th cycle) after which it remained stable. Most likely, the largest degree of side reactions occurred after the
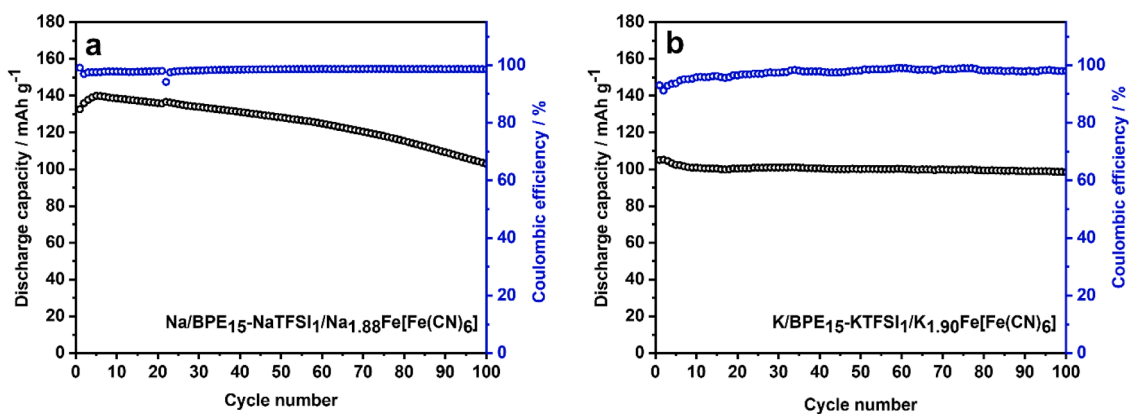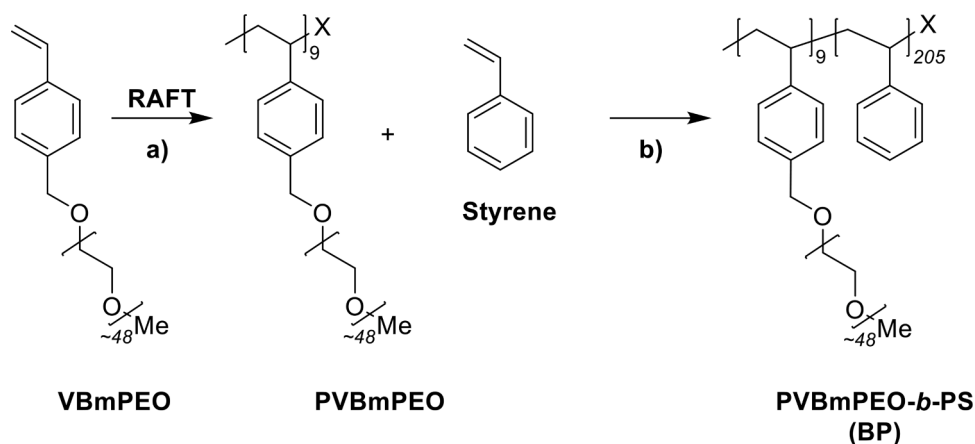
Fig. 7. Capacity retention and corresponding coulombic efficiencies of A/BPE$_{15}$-ATFSI$_1$/A$_{2-x}$Fe[Fe(CN)$_6$] cells where A$_{2-x}$ = (a) Na$_{1.88}$, (b) K$_{1.90}$.

Scheme 1. Block copolymer synthesis by a) polymerizing VBmPEO yielding PVBmPEO as a macro-RAFT agent (X symbolizes the RAFT end group). Subsequently, styrene was used for the chain extension b) yielding PVBmPEO-*b*-PS (BP).

conditioning cycle, eventually leading to the formation of a stable SEI, which is reflected in consistent CE values in the following cycles. As a reference system, NaFF was cycled in a sodium half-cell with carbonate-based liquid electrolyte (see **Experimental section**) at a temperature of 25 °C and a cycling rate of C/10 (**Figure S8c,d**). At these cycling conditions, the cell exhibited a slightly higher capacity retention of 77% over 100 cycles compared to the BPE$_{15}$-NaTFSI$_1$-cell (73%) operated at 55 °C and a C-rate of C/15. Furthermore, compared to the cell with the SPE, the LE-cell showed a significantly lower polarization over the same number of cycles (0.3 V vs. <0.1 V, **Figure S7a and Figure S8c**, respectively). As shown in **Figure S8d**, a larger coulombic efficiency decay (from 96 to 86%) in the first five cycles was observed for the cell with organic LE, followed by further CE increase, reaching a stable value of ~98% in the 50th cycle. These findings could possibly indicate unsuitable cycling conditions, i.e., the temperature and C-rate, for the Na/BPE$_{15}$-NaTFSI$_1$/NaFF cell, leading to its larger polarization and unexpectedly lower capacity retention. To put these results into context, Sångeland et al. reported on the same cell configuration, using poly(trimethylene carbonate) (PTMC)-based PE ((PTMC)$_1$−NaFSI$_1$; σ = 5 × 10^{-5} S cm^{-1} at 25 °C) [70], which achieved a 78% capacity retention over the first 30 cycles at C/5 and at operation temperature of 40 °C. With a slightly altered electrolyte composition (PTMC)$_5$−NaFSI$_1$ a discharge capacity of ~90 mAh g^{-1} over >80 cycles with a 90% capacity retention could be achieved at 60 °C. In a follow-up study by the same authors, polycaprolactone(PCL)–PTMC copolymer was tested in a battery comprising a hard carbon anode and a NaFF cathode [71]. At a temperature of 22 °C and a current density of 10 μA cm^{-2}, the battery showed an initial discharge capacity of 80 mAh g^{-1}, however, with a

continuous fading that resulted in a poor capacity retention of ~50% over 100 cycles. To the best of our knowledge, no other examples of polymer-based sodium cells with NaFF cathodes have been so far reported.

As presented in Fig. 7b, the K-metal/BPE$_{15}$-KTFSI$_1$/KFF cell enabled stable cycling over 100 cycles. A discharge capacity of 105 mAh g^{-1} was obtained in the first cycle followed by a slight increase in the second cycle (105.2 mAh g^{-1}), which is ~75% of theoretical capacity of KFF (141 mAh g^{-1}) and about 90% of the achievable capacity in the same cell configuration with a liquid electrolyte [21]. The most notable capacity decay herein was observed from the 2nd to the 17th cycle, corresponding to a capacity loss of ~5%. This is also reflected in the evolution of the CE, which increased over the same cycle interval from 91.2 to ~97%, indicating a higher degree of irreversible reactions in the first cycles that attenuated in subsequent cycles (Fig. 7b). Notably, after the interfaces were formed, both discharge capacity and CE remained stable over following cycles, resulting in a total capacity retention of 94% and CE of ~98% over 100 cycles. The improved cycling stability is likely an effect of the good mechanical properties of the SPE. For comparison, a potassium cell employing the same cathode material, KFF, but SPE based on pure PEO, i.e., PEO$_{20}$-KTFSI$_1$ [21] exhibited capacity retention of 90% over the first 50 cycles at a temperature of 55 °C and C-rate of C/25. For the BPE$_{15}$-KTFSI$_1$ SPE described herein, the capacity retention was 95% over the same number of cycles and only slightly decreased (94%) at twice the number of cycles. As reported previously, a control experiment in a KFF half cell and a carbonate-based liquid electrolyte retained only 66% of its initial capacity over 50 cycles at a temperature of 20 °C and C-rate of C/25 [21]. Therefore, BPE$_{15}$-KTFSI$_1$

is not only advantageous over conventional carbonate-based LEs but also over solely PEO-based electrolytes. Both SPEs (based on either PEO or BP) approach coulombic efficiencies of around 98% at 55 °C operating temperature, indicating that there is still a significant degree of side reactions. The inefficiencies are probably masked by the vast potassium excess at the counter electrode. It will thus be paramount for the future to target lower operating temperatures.

Recently, Komaba et al. reported a solid-state polymer potassium battery enabled by ether-based cross-linked polymer electrolyte mixed with potassium bis(fluorosulfonyl)amide (KFSA) [72]. At ambient temperature of 25 °C, the PE showed one order of magnitude higher σ_{total} than BPE_{15}-$KTFSI_1$ presented herein ($\sim 3.0 \times 10^{-5}$ vs. 3.9×10^{-6} S cm^{-1}, respectively). Galvanostatic cycling in $K/SPE/K_xFe[Fe(CN)_6]_y$ cells (composition of cathode not further specified) yielded 98% discharge capacity retention over the first 10 cycles, whereas cycling in a full cell configuration, i.e. graphite/SPE/ $K_xFe[Fe(CN)_6]_y$, only resulted in $\sim 30\%$ of discharge capacity retention over the initial 10 cycles at 25 °C. Castillo-Martínez et al. presented a PE comprising PEO and potassium tetraphenylborate ($KBPh_4$) [73]. The PEO_{30}-$(KBPh_4)_1$ composition exhibited total ionic conductivity of 1.1×10^{-4} S cm^{-1} at 55 °C, which is one order of magnitude higher than that of BPE_{15}-$KTFSI_1$ (3.6×10^{-5} S cm^{-1} at 55 °C). In symmetrical 'prussian blue' cells, PEO_{30}-$(KBPh_4)_1$ showed large overpotentials associated with low capacities of only ~ 20 mAh g^{-1} at 80 °C and 45 mAh g^{-1} at 60 °C, respectively.

In summary, BPE_{15}-$Na/KTFSI_1$ presented in this study were successfully employed as SPEs and cycled in sodium/potassium-metal batteries against their respective PBA-based cathode. The high cycling stability of the K-cell can be highlighted, with a capacity retention of 94% over 100 cycles and a maximum capacity of 105.2 mAh g^{-1}, indicating a good interfacial compatibility with the electrodes at the chosen cycling conditions. Meanwhile, the Na-based cell featured a maximum capacity of 140 mAh g^{-1} and retained 73% of its maximum capacity over the same number of cycles. Possibly, the chosen cycling conditions were not ideal for the Na-system, in particular with respect to the operation temperature below 60 °C. This resulted in a larger polarization and overall faster capacity fade compared to the corresponding K-system. We further found that examples of cell tests against established cathode materials are still comparatively rare.

4. Conclusion

In this study, we presented a comprehensive view onto the properties and use of SPEs based on the block copolymer PVBmPEO-*b*-PS (denoted to as block copolymer-based electrolytes, BPE), and the TFSI-salts of Li, Na, and K. As reported previously [22], the microphase-separation of the block copolymer enabled efficient ion transport through the PEO phase, while maintaining high mechanical integrity imparted by the PS phase. Our study revealed dependencies on the choice of cation, i.e., cation size, for the thermal and ion transport properties of the respective SPEs. Specifically, KTFSI-based SPEs showed the lowest T_gs in the entire range of salt concentration investigated (EO:A = 20:1, 15:1, 10:1), indicating the potential of more mobile segmental motion. Amongst the three ion conductors, BPE-KTFSI SPEs displayed the lowest total ionic conductivity (3.95×10^{-6} S cm^{-1} at 25 °C), and BPE-LiTFSI demonstrated the highest one (7.20×10^{-6} S cm^{-1} at 25 °C for BPE_{15}-$LiTFSI_1$). To study how the ion transport is affected by the type and size of cation in more detail, transference number measurements were carried out according to the Bruce-Vincent method. In addition, self-diffusion measurements using PFG NMR were conducted. At 55 °C the BPE-LiTFSI SPE showed a T_{Li}^+ of 0.13 (Bruce-Vincent) and 0.18 (PFG NMR). When attempting to determine values for T_{Na}^+ or T_K^+ no reliable results were obtained, presumably due to the high interfacial resistance in the symmetrical alkali metal-SPE cells. Because of technical constraints, determination of the self-diffusion coefficients by PFG NMR was possible only for the TFSI-anion using the ^{19}F nuclei. This stresses the need to develop novel techniques and methods for the characterization of transport parameters

in post-Li-based PEs.

Notably, all investigated BPE-ATFSI displayed high mechanical strength (G' $\sim 2 \times 10^2$ kPa at 55 °C) and viscoelastic solid-like behavior that is highly desirable for PEs in alkali metal batteries, particularly when operated at elevated temperatures.

Plating and stripping experiments in Na-Na and K-K symmetrical cells displayed almost 10 times larger overpotentials than corresponding Li-Li-cells under same experimental conditions. For full cell tests, either BPE_{15}-$NaTFSI_1$ or BPE_{15}-$KTFSI_1$ SPEs were implemented in alkali metal batteries with the respective metal negative electrode and a PBA ($A_{2-x}Fe$ $[Fe(CN)_6]$) positive electrode that were cycled at 55 °C and at a cycling rate of C/15. The $Na/SPE/Na_{1.88}Fe[Fe(CN)_6]$ cell showed a capacity retention of $\sim 73\%$ over 100 cycles with an initial discharge capacity of 140 mAh g^{-1}. Under similar conditions, the $K/SPE/K_{1.90}Fe[Fe(CN)_6]$ full cell showed better capacity retention of 94% over 100 cycles at an initial capacity of 105 mAh g^{-1}. The coulombic efficiencies in both cell setups were about 98% at the 100th cycle, which clearly shows that at elevated temperatures and in contact with reactive alkali metals as negative electrode, side reactions occur to a considerable extent. When compared to a liquid electrolyte system and our previously published PEO-KTFSI SPEs, BPE-KTFSI compositions showed higher mechanical rigidity, especially at the relevant operation temperatures, and considerably improved capacity retention over the first 100 cycles in the same cell configuration. Our results highlight that promising results can be achieved when combining material properties in a block copolymer approach for polymer electrolytes in post-Li battery applications.

CRediT authorship contribution statement

Anna D. Khudyshkina: Methodology, Investigation, Validation, Data curation, Writing – original draft, Writing – review & editing, Visualization. **Andreas J. Butzelaar:** Methodology, Investigation, Validation, Writing – original draft, Writing – review & editing. **Yiran Guo:** Investigation, Validation, Writing – original draft. **Maxi Hoffmann:** Methodology, Investigation, Validation, Writing – original draft, Writing – review & editing. **Thomas Bergfeldt:** Methodology, Investigation, Validation, Writing – review & editing. **Mareen Schaller:** Methodology, Investigation, Validation, Writing – original draft, Writing – review & editing, Visualization. **Sylvio Indris:** Methodology, Writing – review & editing. **Manfred Wilhelm:** Writing – review & editing, Supervision. **Patrick Théato:** Conceptualization, Writing – review & editing, Supervision. **Fabian Jeschull:** Conceptualization, Software, Writing – original draft, Writing – review & editing, Supervision.

Declaration of Competing Interest

The authors declare that they have no known competing financial interests or personal relationships that could have appeared to influence the work reported in this paper. The data to the above presented findings are available on Zenodo online repository DOI: 10.5281/zenodo.7428858 [74]. The R package 'bat2dat' was used for processing galvanostatic cycling data, ref [27].

Acknowledgements

acknowledged for proofreading as a native speaker.

Supplementary materials

Supplementary material associated with this article can be found, in the online version, at doi:10.1016/j.electacta.2023.142421.

References

[1] H. Wang, D. Yu, C. Kuang, L. Cheng, W. Li, X. Feng, Z. Zhang, X. Zhang, Y. Zhang, Alkali metal anodes for rechargeable batteries, Chem 5 (2019) 313–338, https://doi.org/10.1016/J.CHEMPR.2018.11.005.

[2] X. Min, J. Xiao, M. Fang, W. Wang, Y. Zhao, Y. Liu, A.M. Abdelkader, K. Xi, R. V. Kumar, Z. Huang, Potassium-ion batteries: outlook on present and future technologies, Energy Environ. Sci. 14 (2021) 2186–2243, https://doi.org/10.1039/D0EE02917C.

[3] B. John, V. Anoopkumar, T.D. Mercy, Potassium-ion batteries: key to future large-scale energy storage? ACS Appl. Energy Mater. 3 (2020) 9478–9492, https://doi.org/10.1021/acsaem.0c01574.

[4] C. Vaalma, D. Buchholz, M. Weil, S. Passerini, A cost and resource analysis of sodium-ion batteries, Nat. Rev. Mater. 3 (2018) 18013, https://doi.org/10.1038/natrevmats.2018.13.

[5] K. Kubota, M. Dahbi, T. Hosaka, S. Kumakura, S. Komaba, Towards K-ion and Na-ion batteries as "beyond Li-ion, Chem. Rec. 18 (2018) 459–479, https://doi.org/10.1002/tcr.201700057.

[6] X. Bie, K. Kubota, T. Hosaka, K. Chihara, S. Komaba, A novel K-ion battery: hexacyanoferrate(ii)/graphite cell, J. Mater. Chem. A. 5 (2017) 4325–4330, https://doi.org/10.1039/c7ta00220c.

[7] S. Zhao, Z. Guo, K. Yan, X. Guo, S. Wan, F. He, B. Sun, G. Wang, The rise of prussian blue analogs: challenges and opportunities for high-performance cathode materials in potassium-ion batteries, Small Struct. 2 (2021), 2000054, https://doi.org/10.1002/SSTR.202000054.

[8] S.S. Fedotov, N.R. Khasanova, A.S. Samarin, O.A. Drozhzhin, D. Batuk, O. M. Karakulina, J. Hadermann, A.M. Abakumov, E.V. A.ntipov, AVPO 4 F (A = Li, K): a 4V cathode material for high-power rechargeable batteries, Chem. Mater. 28 (2016) 411–415, https://doi.org/10.1021/acs.chemmater.5b04065.

[9] J. Xiao, X. Li, K. Tang, D. Wang, M. Long, H. Gao, W. Chen, C. Liu, H. Liu, G. Wang, Recent progress of emerging cathode materials for sodium ion batteries, Mater. Chem. Front. 5 (2021) 3735–3764, https://doi.org/10.1039/D1QM00179E.

[10] T. Hosaka, K. Kubota, A.S. Hameed, S. Komaba, Research development on K-ion batteries, Chem. Rev. 120 (2020) 6358–6466, https://doi.org/10.1021/acs.chemrev.9b00463.

[11] D. Lin, Y. Liu, Y. Cui, Reviving the lithium metal anode for high-energy batteries, Nat. Nanotechnol. 123 (12) (2017) 194–206, https://doi.org/10.1038/nnano.2017.16, 2017.

[12] X.B. Cheng, R. Zhang, C.Z. Zhao, Q. Zhang, Toward safe lithium metal anode in rechargeable batteries: a review, Chem. Rev. 117 (2017) 10403–10473, https://doi.org/10.1021/ACS.CHEMREV.7B00115.

[13] S. Liu, S. Tang, X. Zhang, A. Wang, Q.H. Yang, J. Luo, Porous Al current collector for dendrite-free Na metal anodes, Nano Lett. 17 (2017) 5862–5868, https://doi.org/10.1021/ACS.NANOLETT.7B03185.

[14] G. Homann, L. Stolz, J. Nair, I.C. Laskovic, M. Winter, J. Kasnatscheew, Poly (ethylene oxide)-based electrolyte for solid-state-lithium-batteries with high voltage positive electrodes: evaluating the role of electrolyte oxidation in rapid cell failure, Sci. Rep. 10 (2020) 1–9, https://doi.org/10.1038/s41598-020-61373-9.

[15] G. Homann, L. Stolz, K. Neuhaus, M. Winter, J. Kasnatscheew, Effective optimization of high voltage solid-state lithium batteries by using poly(ethylene oxide)-based polymer electrolyte with semi-interpenetrating network, Adv. Funct. Mater. 30 (2020), 2006289, https://doi.org/10.1002/ADFM.202006289.

[16] G. Homann, L. Stolz, M. Winter, J. Kasnatscheew, Elimination of "voltage noise" of poly (ethylene oxide)-based solid electrolytes in high-voltage lithium batteries: linear versus network polymers, IScience 23 (2020), 101225, https://doi.org/10.1016/j.isci.2020.101225.

[17] L. Frenck, G.K. Sethi, J.A. Maslyn, N.P. Balsara, Factors that control the formation of dendrites and other morphologies on lithium metal anodes, Front. Energy Res. 7 (2019) 115, https://doi.org/10.3389/FENRG.2019.00115.

[18] D. Cao, X. Sun, Q. Li, A. Natan, P. Xiang, H. Zhu, Lithium dendrite in all-solid-state batteries: growth mechanisms, suppression strategies, and characterizations, Matter 3 (2020) 57–94, https://doi.org/10.1016/J.MATT.2020.03.015.

[19] H. Zhang, Y. Chen, C. Li, M. Armand, C.Heng Zhang, Electrolyte and anode-electrolyte interphase in solid-state lithium metal polymer batteries: a perspective, SusMat 1 (2021) 24–37, https://doi.org/10.1002/SUS2.6.

[20] J. Mindemark, M.J. Lacey, T. Bowden, D. Brandell, Beyond PEO—alternative host materials for Li + -conducting solid polymer electrolytes, Prog. Polym. Sci. 81 (2018) 114–143, https://doi.org/10.1016/j.progpolymsci.2017.12.004.

[21] A.D. Khudyshkina, P.A. Morozova, A.J. Butzelaar, M. Hoffmann, M. Wilhelm, P. Theato, S.S. Fedotov, F. Jeschull, Poly(ethylene oxide)-based electrolytes for solid-state potassium metal batteries with a prussian blue positive electrode, ACS Appl. Polym. Mater. 4 (2022) 2734–2746, https://doi.org/10.1021/acsapm.2c00014.

[22] A.J. Butzelaar, P. Röring, T.P. Mach, M. Hoffmann, F. Jeschull, M. Wilhelm, M. Winter, G. Brunklaus, P. Théato, Styrene-based poly(ethylene oxide) side-chain block copolymers as solid polymer electrolytes for high-voltage lithium-metal

[23] U. Oteo, M. Martinez-Ibañez, I. Aldalur, E. Sanchez-Diez, J. Carrasco, M. Armand, H. Zhang, Improvement of the cationic transport in polymer electrolytes with (difluoromethanesulfonyl)(trifluoromethanesulfonyl)imide Salts, ChemElectroChem 6 (2019) 1019–1022, https://doi.org/10.1002/celc.201801472.

[24] A. Memboeuf, A., Vékey, K., Lendvay, G. Structure and energetics of poly(ethylene glycol) cationized by Li+, Na+, K+ and Cs+: a first-principles study:, Http://Dx. Doi.Org/10.1255/Ejms.1107. 17 (2011) 33–46. doi:10.1255/EJMS.1107.

[25] L. Poudel, R. Podgornik, W.Y. Ching, The hydration effect and selectivity of alkali metal ions on poly(ethylene glycol) models in cyclic and linear topology, J. Phys. Chem. A. 121 (2017) 4721–4731, https://doi.org/10.1021/ACS.JPCA.7B04061.

[26] V. St-Onge, S. Rochon, J.C. Daigle, A. Soldera, J.P. Claverie, The unusual conductivity of Na+ in PEO-based statistical copolymer solid electrolytes: when less means more, Angew. Chemie Int. Ed. 60 (2021) 25897–25904, https://doi.org/10.1002/ANIE.202109709.

[27] Jeschull, F. bat2dat_v1.0.1, (2022). doi:10.5281/zenodo.7439377.

[28] Y.W. Kim, W. Lee, B.K. Choi, Relation between glass transition and melting of PEO-salt complexes, Electrochim. Acta. 45 (2000) 1473–1477, https://doi.org/10.1016/S0013-4686(99)00362-X.

[29] R. He, T. Kyu, Effect of plasticization on ionic conductivity enhancement in relation to glass transition temperature of crosslinked polymer electrolyte membranes, Macromolecules 49 (2016) 5637–5648, https://doi.org/10.1021/ACS.MACROMOL.6B00918.

[30] D.J. Brooks, B.V. M.erinov, I. William A. Goddard, B. Kozinsky, J. Mailoa, Atomistic description of ionic diffusion in PEO–LiTFSI: effect of temperature, molecular weight, and ionic concentration, Macromolecules 51 (2018) 8987–8995, https://doi.org/10.1021/ACS.MACROMOL.8B01753.

[31] C. Monroe, J. Newman, The impact of elastic deformation on deposition kinetics at lithium/polymer interfaces, J. Electrochem. Soc. 152 (2005) A396, https://doi.org/10.1149/1.1850854.

[32] G. Dreezen, M.H.J. Koch, H. Reynaers, G. Groeninckx, Miscible binary blends of poly(ethylene oxide) and an amorphous aromatic polyamide (Aramide 34I): crystallization, melting behavior and semi-crystalline morphology, Polymer (Guildf) 40 (1999) 6451–6463, https://doi.org/10.1016/S0032-3861(98)00849-0.

[33] J.F. Le Nest, A. Gandini, H. Cheradame, J.P. Cohen-Addad, Influence of LiClO4on the properties of polyether networks: specific volume and glass transition temperature, Macromolecules 21 (1988) 1117–1120, https://doi.org/10.1021/ma00182a044.

[34] G. Mao, R.F. Perea, W.S. Howells, D.L. Price, M.-.L. Saboungi, Relaxation in polymer electrolytes on the nanosecond timescale, Nat 405 (2000) 163–165, https://doi.org/10.1038/35012032, 2000 4056783.

[35] A.J. Butzelaar, K.L. Liu, P. Röring, G. Brunklaus, M. Winter, P. Theato, A systematic study of vinyl ether-based poly(ethylene oxide) side-chain polymer electrolytes, ACS Appl. Polym. Mater. 3 (2021) 1573–1582, https://doi.org/10.1021/acsapm.0c01398.

[36] R.D. Shannon, Revised effective ionic radii and systematic studies of interatomic distances in halides and chalcogenides, Acta Cryst 32 (1976) 751–767, https://doi.org/10.1107/S0567739476001551.

[37] J.B. Thomson, P. Lightfoot, P.G. Bruce, Structure of polymer electrolytes: the crystal structure of poly(ethylene oxide)4:RbSCN, Solid State Ionics 85 (1996) 203–208, https://doi.org/10.1016/0167-2738(96)00060-4.

[38] J.H. Shin, W.A. Henderson, S. Passerini, Ionic liquids to the rescue? Overcoming the ionic conductivity limitations of polymer electrolytes, Electrochem. Commun. 5 (2003) 1016–1020, https://doi.org/10.1016/j.elecom.2003.09.017.

[39] S. Lascaud, M. Perrier, A. Vallée, S. Besner, J. Prud'homme, M. Armand, Phase diagrams and conductivity behavior of poly(ethylene oxide)-molten salt rubbery electrolytes, Macromolecules 27 (1994) 7469–7477, https://doi.org/10.1021/ma00103a034.

[40] M. Perrier, S. Besner, C. Paquette, A. Vallée, S. Lascaud, J. Prud'homme, Mixed-alkali effect and short-range interactions in amorphous poly(ethylene oxide) electrolytes, Electrochim. Acta. 40 (1995) 2123–2129, https://doi.org/10.1016/0013-4686(95)00151-4.

[41] M. Marzantowicz, J.R. Dygas, F. Krok, J.L. Nowiński, A. Tomaszewska, Z. Florjańczyk, E. Zygadło-Monikowska, Crystalline phases, morphology and conductivity of PEO:LiTFSI electrolytes in the eutectic region, J. Power Sources. 159 (2006) 420–430, https://doi.org/10.1016/J.JPOWSOUR.2006.02.044.

[42] J. Lopez, D.G. Mackanic, Y. Cui, Z. Bao, Designing polymers for advanced battery chemistries, Nat. Rev. Mater. 45 (4) (2019) 312–330, https://doi.org/10.1038/s41578-019-0103-6, 2019.

[43] Z. Xue, D. He, X. Xie, Poly(ethylene oxide)-based electrolytes for lithium-ion batteries, J. Mater. Chem. A. 3 (2015) 19218–19253, https://doi.org/10.1039/C5TA03471J.

[44] M. Worzakowska, Thermal and mechanical properties of polystyrene modified with esters derivatives of 3-phenylprop-2-en-1-ol, J. Therm. Anal. Calorim. 121 (2015) 235–243, https://doi.org/10.1007/S10973-015-4547-7.

[45] L. Stolz, S. Röser, G. Homann, M. Winter, J. Kasnatscheew, Pragmatic approaches to correlate between the physicochemical properties of a linear poly(ethylene oxide)-based solid polymer electrolyte and the performance in a high-voltage Li-metal battery, J. Phys. Chem. C. 125 (2021) 18089–18097, https://doi.org/10.1021/ACS.JPCC.1C03614.

[46] M. Singh, O. Odusanya, G.M. Wilmes, H.B. Eitouni, E.D. Gomez, A.J. Patel, V. L. Chen, M.J. Park, P. Fragouli, H. Iatrou, N. Hadjichristidis, D. Cookson, N. P. Balsara, Effect of molecular weight on the mechanical and electrical properties

batteries, ACS Appl. Mater. Interfaces. 13 (2021) 39257–39270, https://doi.org/10.1021/acsami.1c08841.

of block copolymer electrolytes, Macromolecules 40 (2007) 4578–4585, https://doi.org/10.1021/ma0629541.

[47] Harun, F., Chan, C.H., Guo, Q. Rheology and microscopic heterogeneity of poly (ethylene oxide) solid polymer electrolytes, (2017). doi:10.1002/masy.201700040.

[48] J. Lopez, D.G. Mackanic, Y. Cui, Z. Bao, Designing polymers for advanced battery chemistries, Nat. Rev. Mater. 4 (2019) 312–330, https://doi.org/10.1038/s41578-019-0103-6.

[49] A. Maurel, M. Armand, S. Grugeon, B. Fleutot, C. Davoisne, H. Tortajada, M. Courty, S. Panier, L. Dupont, Poly(ethylene oxide) solid polymer electrolyte filaments for fused deposition modeling three-dimensional printing, J. Electrochem. Soc. 167 (2020) 070536, https://doi.org/10.1149/1945-7111/AB7C38.

[50] S.B. Aziz, T.J. Woo, M.F.Z. Kadir, H.M. Ahmed, A conceptual review on polymer electrolytes and ion transport models, J. Sci. Adv. Mater. Devices. 3 (2018) 1–17, https://doi.org/10.1016/J.JSAMD.2018.01.002.

[51] M. Jaipal Reddy, T. Sreekanth, U.V. S.ubba Rao, Study of the plasticizer effect on a (PEO + NaYF4) polymer electrolyte and its use in an electrochemical cell, Solid State Ionics 126 (1999) 55–63, https://doi.org/10.1016/S0167-2738(99)00225-8.

[52] A.J. Butzelaar, P. Röring, M. Hoffmann, J. Atik, E. Paillard, M. Wilhelm, M. Winter, G. Brunklaus, P. Theato, Advanced block copolymer design for polymer electrolytes: prospects of microphase separation, Macromolecules 54 (2021) 11101–11112, https://doi.org/10.1021/ACS.MACROMOL.1C02147.

[53] J. Evans, C.A. Vincent, P.G. Bruce, Electrochemical measurement of transference numbers in polymer electrolytes, Polymer (Guildf) 28 (1987) 2324–2328, https://doi.org/10.1016/0032-3861(87)90394-6.

[54] F. Allgayer, J. Maibach, F. Jeschull, Comparing the solid electrolyte interphases on graphite electrodes in K and Li half cells, ACS Appl. Energy Mater. 5 (2022) 1136–1148, https://doi.org/10.1021/acsaem.1c03491.

[55] D. Brandell, J. Mindemark, G. Hernández, Polymer-Based Solid State Batteries, De Gruyter, BostonBerlin, 2021, https://doi.org/10.1515/9781501521140/HTML.

[56] R. Dugas, J.D. Forero-Saboya, A. Ponrouch, Methods and protocols for reliable electrochemical testing in post-Li batteries (Na, K, Mg, and Ca), Chem. Mater. 31 (2019) 8613–8628, https://doi.org/10.1021/acs.chemmater.9b02776.

[57] A. Boschin, M.E. Abdelhamid, P. Johansson, On the feasibility of sodium metal as pseudo-reference electrode in solid state electrochemical cells, ChemElectroChem 4 (2017) 2717–2721, https://doi.org/10.1002/CELC.201700273.

[58] E.O. Stejskal, J.E. Tanner, Spin diffusion measurements: spin echoes in the presence of a time-dependent field gradient, J. Chem. Phys. 42 (2004) 288, https://doi.org/10.1063/1.1695690.

[59] H. Wang, D. Zhai, F. Kang, Solid electrolyte interphase (SEI) in potassium ion batteries, Energy Environ. Sci. 13 (2020) 4583–4608, https://doi.org/10.1039/D0EE01638A.

[60] J. Chen, C. Wang, G. Wang, D. Zhou, L.-.Z. Fan, An interpenetrating network polycarbonate-based composite electrolyte for high-voltage all-solid-state lithium-metal batteries, Energy Mater. 2 (2022) 200023, https://doi.org/10.20517/ENERGYMATER.2022.25.

[61] T. Huang, G. Du, Y. Qi, J. Li, W. Zhong, Q. Yang, X. Zhang, M. Xu, A Prussian blue analogue as a long-life cathode for liquid-state and solid-state sodium-ion batteries, Inorg. Chem. Front. 7 (2020) 3938–3944, https://doi.org/10.1039/D0QI00872A.

[62] X. Bie, K. Kubota, T. Hosaka, K. Chihara, S. Komaba, A novel K-ion battery: hexacyanoferrate(II)/graphite cell, J. Mater. Chem. A. 5 (2017) 4325–4330, https://doi.org/10.1039/C7TA00220C.

[63] H. Kim, H. Ji, J. Wang, G. Ceder, Next-generation cathode materials for non-aqueous potassium-ion batteries, Trends Chem. 1 (2019) 682–692, https://doi.org/10.1016/j.trechm.2019.04.007.

[64] S. Komaba, T. Hasegawa, M. Dahbi, K. Kubota, Potassium intercalation into graphite to realize high-voltage/high-power potassium-ion batteries and potassium-ion capacitors, Electrochem. Commun. 60 (2015) 172–175, https://doi.org/10.1016/j.elecom.2015.09.002.

[65] G. Hernández, I.L. Johansson, A. Mathew, C. Sångeland, D. Brandell, J. Mindemark, Going beyond sweep voltammetry: alternative approaches in search of the elusive electrochemical stability of polymer electrolytes, J. Electrochem. Soc. 168 (2021), 100523, https://doi.org/10.1149/1945-7111/AC2D8B.

[66] H. Fei, Y. Liu, Y. An, X. Xu, J. Zhang, B. Xi, S. Xiong, J. Feng, Safe all-solid-state potassium batteries with three dimentional, flexible and binder-free metal sulfide array electrode, J. Power Sources. 433 (2019) 226697, https://doi.org/10.1016/j.jpowsour.2019.226697.

[67] W.R. Brant, R. Mogensen, S. Colbin, D.O. Ojwang, S. Schmid, L. Häggström, T. Ericsson, A. Jaworski, A.J. Pell, R. Younesi, Selective control of composition in prussian white for enhanced material properties, Chem. Mater. 31 (2019) 7203–7211, https://doi.org/10.1021/acs.chemmater.9b01494.

[68] T. Hosaka, T. Fukabori, H. Kojima, K. Kubota, S. Komaba, Effect of particle size and anion vacancy on electrochemical potassium ion insertion into potassium manganese hexacyanoferrates, ChemSusChem 14 (2021) 1166–1175, https://doi.org/10.1002/cssc.202002628.

[69] J. Cattermull, M. Pasta, A.L. Goodwin, Structural complexity in Prussian blue analogues, Mater. Horizons. 8 (2021) 3178–3186, https://doi.org/10.1039/d1mh01124c.

[70] C. Sångeland, R. Mogensen, D. Brandell, J. Mindemark, Stable cycling of sodium metal all-solid-state batteries with polycarbonate-based polymer electrolytes, ACS Appl. Polym. Mater. 1 (2019) 825–832, https://doi.org/10.1021/acsapm.9b00068.

[71] C. Sångeland, R. Younesi, J. Mindemark, D. Brandell, Towards room temperature operation of all-solid-state Na-ion batteries through polyester–polycarbonate-based polymer electrolytes, Energy Storage Mater. 19 (2019) 31–38, https://doi.org/10.1016/j.ensm.2019.03.022.

[72] M. Hamada, R. Tatara, K. Kubota, S. Kumakura, S. Komaba, All-solid-state potassium polymer batteries enabled by the effective pretreatment of potassium metal, ACS Energy Lett. 7 (2022) 2244–2246, https://doi.org/10.1021/acsenergylett.2c01096.

[73] M. Elmanzalawy, E. Sanchez-Ahijón, O. Kisacik, J. Carretero-González, E. Castillo-Martínez, High conductivity in a fluorine-free K-ion polymer electrolyte, ACS Appl. Energy Mater. 5 (2022) 9009–9019, https://doi.org/10.1021/acsaem.2c01485.

[74] A.D. Khudyshkina, A.J. Butzelaar, Y. Guo, M. Hoffmann, T. Bergfeldt, M. Schaller, S. Indris, M. Wilhelm, P. Theato, F. Jeschull, Datasets to from lithium to potassium: comparison of cations in poly(ethylene oxide)-based block copolymer electrolytes for solid-state alkali metal batteries, Zenodo Online Repos (2023), https://doi.org/10.5281/zenodo.7428858.